

1 **Future tropospheric ozone budget and distribution over** 2 **East Asia under a Net Zero scenario**

3 Xuewei Hou^{1,4}, Oliver Wild², Bin Zhu¹, James Lee³

4 ¹Collaborative Innovation Center on Forecast and Evaluation of Meteorological Disasters, Key
5 Laboratory of Meteorological Disaster, Ministry of Education (KLME), School of Atmospheric
6 Physics, Nanjing University of Information Science and Technology, Nanjing, China

7 ²Lancaster Environment Centre, Lancaster University, Lancaster, UK

8 ³Department of Chemistry, University of York, York, UK

9 ⁴Key Laboratory of Atmospheric Chemistry, China Meteorological Administration, Beijing
10 (LAC/CMA), China

11 *Correspondence to:* Xuewei Hou (houxw@nuist.edu.cn)

12 **Abstract:** Under future net zero emission policies, reductions in emissions of ozone (O₃) precursors are
13 expected to alter the temporal and spatial distribution of tropospheric O₃. In this study, we quantify
14 changes in the tropospheric O₃ budget, spatiotemporal distribution of surface O₃ in East Asia and the
15 contributions from regional emissions, intercontinental transport and climate change between the present
16 day and 2060 under a net zero scenario, using the NCAR Community Earth System Model (CESM) with
17 online tagging of O₃ and its precursors. The results reveal that the global tropospheric O₃ burden is likely
18 to decrease by more than 20%, from 316 Tg in present day to 247 Tg in 2060, under a net zero scenario.
19 The burden of stratospheric O₃ in the troposphere is expected to increase from 69 to 77 Tg. The mean
20 lifetime of tropospheric O₃ increases by 2 days, ~10%. Changes in climate under a net zero pathway are
21 relatively small, and only lead to small increases in tropospheric O₃. Over East China, surface O₃
22 increases in winter, due to the weakened titration of O₃ by NO associated with reduced anthropogenic
23 NO emissions, and to enhanced stratospheric input. In summer, surface O₃ decreases by more than 30
24 ppbv, and peak concentrations shift from July to May. Local contributions from anthropogenic emissions
25 to surface O₃ over East Asia are highest in summer, but drop substantially, from 30% to 14%, under a
26 net zero scenario. The contribution of biogenic NO sources is enhanced, and forms the dominant
27 contributor to future surface O₃, especially in summer, ~40%. This enhanced contribution is mainly due
28 to the increased O₃ production efficiency under lower anthropogenic precursor emissions. Over Eastern
29 China, local anthropogenic contributions decrease from 50% to 30%. The decreases in surface O₃ are
30 strongly beneficial, and are more than sufficient to counteract the increases in surface O₃ observed in
31 China over recent years. This study thus highlights the important co-benefits of net zero policies that
32 target climate change in addressing surface O₃ pollution over East Asia.

33 **Keywords:** Tropospheric O₃; SSP1-1.9 pathway; net zero; O₃ budgets; stratospheric contribution

34 **1 Introduction**

35 Although ozone (O₃) occurs naturally in small quantities in the lower troposphere, unhealthy levels of
36 tropospheric O₃ are created when high levels of anthropogenic pollutants, such as nitrogen oxides (NO_x),
37 and volatile organic compounds (VOCs) are oxidized in the presence of solar radiation. This excess O₃
38 acts as a pollutant and greenhouse gas, contributing to harmful smog that damages human health and
39 ecosystems (Jerrett et al., 2009; Malley et al., 2017; Emberson, 2020) and contributing to higher
40 tropospheric temperatures (Myhre et al., 2013; Stevenson et al., 2013). The relatively short lifetime of
41 O₃ in the troposphere (~3 weeks, Young et al., 2013) means that it is classified as a Near Term Climate
42 Forcer (NTCF), having an important influence on climate over shorter timescales than the long-lived
43 greenhouse gases such as CO₂. Tropospheric O₃ is also an oxidant and a precursor for the hydroxyl (OH)
44 radical (Griffiths et al., 2021). OH (and by implication O₃) controls the lifetime of methane (Voulgarakis
45 et al., 2013), the second most important anthropogenic greenhouse gas after carbon dioxide (Myhre et
46 al., 2013). Oxidant levels mediate the formation of secondary aerosols such as sulfate and nitrate and
47 play a major role in the aerosol budget and burden with important consequences for radiative forcing
48 (Shindell et al., 2009; Karset et al., 2018). Understanding how tropospheric O₃ changes is important for
49 both future air quality and climate (Turnock et al., 2019).

50 A multi-model assessment of future changes in tropospheric O₃ was made in the Atmospheric Chemistry
51 and Climate Model Intercomparison Project (ACCMIP), using future changes in climate and O₃ precursor
52 emissions from the Representative Concentration Pathways (RCPs) (Lamarque et al., 2013). The models
53 participating in ACCMIP projected changes in global annual mean surface O₃ concentrations between
54 2000 and 2030 of ±1.5 ppbv under the different RCPs (Young et al., 2013). More recent single model
55 estimates by O'Connor et al. (2014) and Kim et al. (2015) predict surface O₃ responses across the different
56 RCPs of between -4.0 and +2.0 ppbv by 2050 relative to 2000. The global annual mean tropospheric O₃
57 burden was projected to change by between -18% and +20% from 2000 to 2100 under the different RCPs
58 (Cionni et al., 2011; Kawase et al., 2011; O'Connor et al., 2014; Young et al., 2013). Whether
59 tropospheric O₃ increases or decreases in future is dependent on the climate mitigation measures and air
60 pollution policies that are implemented. In preparation for the sixth Coupled Model Intercomparison
61 Project (CMIP6), a new set of future pathways were created. Five different socio-economic pathways
62 (SSPs) were developed with centennial trends based on different combinations of social, economic and
63 environmental developments (O'Neill et al., 2014). Different levels of emissions mitigation were
64 included within each SSP to meet particular climate and air pollution targets (Rao et al., 2017; Riahi
65 et al., 2017). They incorporate stronger links between socio-economic development patterns and climate
66 change risks than previous assessments and provide better hypothetical scenarios for future projections.
67 The five most widely-used scenarios are SSP1-1.9, SSP1-2.6, SSP2-4.5, SSP3-7.0, and SSP5-8.5, where
68 SSP1-SSP5 represent differing socio-economic pathways and the suffix 1.9~8.5 indicates the total
69 radiative forcing (W/m²) at the end of the 21st century compared with that before the Industrial
70 Revolution. These pathways provide a good foundation for assessment of air quality, radiative forcing,
71 ecological environmental effects and human health effects in the future. Many studies have focused on
72 the pessimistic SSP3-7.0 scenario reflecting regional rivalry, and Griffiths et al. (2021) demonstrates that

73 the tropospheric O₃ burden increases from 356 ± 31 Tg in present day to 416 ± 35 Tg in 2100 under this
74 pathway. Liu et al. (2022) shows that the tropospheric O₃ burden increases by 4 % between 2010 and
75 2050 under SSP3-7.0. Based on multi-model simulations conducted for the Aerosol and Chemistry
76 Model Intercomparison Project (AerChemMIP), Allen et al. (2020) and Zanis et al. (2022) reveal a global
77 surface O₃ decrease in future along the SSP3-7.0 scenario, due to enhanced ozone destruction from higher
78 water vapor abundances under a warmer climate. The sustainability-focused SSP1-1.9 pathway is the
79 scenario mostly closely aligned with recent pledges aiming at net zero greenhouse gas emissions, limiting
80 warming to 1.5°C by 2100, but the impacts of this pathway on tropospheric O₃ are less well studied and
81 remain unclear.

82 In East Asia, surface O₃ has increased rapidly since 2000 (Lu et al., 2020), and is expected to increase
83 by another ~10 ppbv by 2050 following the IPCC A1B (Wang et al., 2013), RCP6.0 (Zhu and Liao, 2016)
84 and RCP4.5 (Hong et al., 2019) scenarios. In September 2020, China committed to achieve carbon
85 neutrality by 2060, following the commitments of many developed countries to achieve net zero
86 emissions by 2050. The effect of these strong mitigation measures on surface O₃ has not been explored
87 thoroughly, but the proposed emission pathway to net zero loosely aligns with the SSP1-1.9 pathway.
88 Turnock et al (2019) showed large reductions of >8 ppbv in surface O₃ over East Asia by 2050 along this
89 pathway due to large reductions in precursor emissions and CH₄. The study also shows that any benefits
90 to surface O₃ from reducing local emission sources over East Asia could be offset by intercontinental
91 transport of O₃ formed from sources remote to the region and from global CH₄ sources. This analysis
92 used an O₃ parameterization to rapidly assess changes in O₃ and source attribution (Wild et al., 2012;
93 Turnock et al., 2018), which did not account for changes in climate, stratosphere-to-troposphere
94 exchange, or chemical regime. Other recent assessments exploring the implications of carbon neutrality
95 in China have suggested that O₃ concentrations may decline to 63-94 µg m⁻³ by 2060 (Shi et al., 2021;
96 Wang and Liao, 2022; Xu et al., 2022). The differences between these results have been attributed to the
97 emission and climate scenarios used. Wang and Liao (2022) also found that the annual mean contribution
98 of Southeast Asia to surface MDA8 O₃ in China is 3-19 µg m⁻³, about 2-10 ppbv, and this contribution
99 is reduced in future along the SSP1-1.9 pathway.

100 While previous studies have quantified possible changes in surface O₃ under carbon neutrality, the wider
101 impact on the global tropospheric O₃ budget and the changing contributions of different sources remain
102 unclear. In this study, we quantify the changes in surface O₃ over East Asia, and especially over Eastern
103 China which currently has high anthropogenic emissions, and the contribution of different sources based
104 on emissions and climate change along the SSP1-1.9 pathway, using the NCAR Community Earth
105 System Model (CESM) with online tagging of O₃ and its precursors. We present a self-consistent
106 assessment of the changes in surface O₃ associated with changes in emissions and climate, along with
107 the first attribution of these changes. The paper is organized as follows. Section 2 describes the model
108 configurations, experimental settings, O₃ tagging method, and evaluation datasets. In section 3, O₃ and
109 NO_x in present day simulations is evaluated against observations. In section 4, changes in tropospheric
110 O₃ under the net zero scenario are presented. In section 5, the contribution of O₃ chemistry and

111 intercontinental transport are discussed under present day and future conditions. We close with a
112 summary in section 6.

113 **2 Materials and methods**

114 **2.1 Model configurations and experiments**

115 The NCAR CESM is a coupled climate model incorporating components for simulating the Earth's
116 atmosphere, ocean, land, land-ice, and sea-ice (e.g., Neale et al., 2013; Lamarque et al., 2012; Tilmes et
117 al., 2015; Danabasoglu et al., 2020), allowing fundamental research into the Earth's past, present, and
118 future climate states. CESM showed excellent performance in CMIP6 (Eyring et al., 2016; Fan et al.,
119 2020; Yang et al., 2021). The experiments here use CESM version 1.2.2
120 (<https://www.cesm.ucar.edu/models/cesm1.2/>) and the latest version 2.2.0
121 (<https://www.cesm.ucar.edu/models/cesm2/>), to reproduce present-day O₃ mixing ratios and to predict
122 O₃ responses to emissions and climate in the future along the SSP1-1.9 pathway. All model simulations
123 are performed with prescribed sea surface temperatures and sea ice distribution data for climatological
124 conditions in present day and future net zero, since we focus on the atmospheric component. Dry
125 deposition of gases and aerosols are implemented in the Community Land Model (Oleson, 2010) as
126 described in Lamarque et al. (2012).

127 Atmospheric chemistry of gas phase and aerosol species in the global Community Atmosphere Model
128 (CAM version 4, Neale et al., 2013; CAM version 6, Danabasoglu et al., 2020), the atmospheric
129 component of CESM, is represented by CAM-chem. CAM-chem provides the flexibility of using the
130 same code to perform climate simulations (online) and simulations with specified meteorological fields
131 (offline). The chemical mechanism is based on the Model for Ozone and Related chemical Tracers
132 (MOZART), version 4 mechanism for the troposphere (Emmons et al., 2010), extended for stratospheric
133 chemistry (Kinnison et al., 2007), with further updates as described in Lamarque et al. (2012), including
134 additional reaction rate updates following JPL-2010 recommendations (Sander et al., 2011).

135 In this paper, offline simulations are used to investigate the effect of emission changes on tropospheric
136 O₃ under fixed meteorological parameters, while online simulations are used for the effects of emission
137 and climate changes with two-way feedback of atmospheric components and meteorological parameters.
138 Two different versions of CESM are used in this study due to the application of online tagging of O₃ and
139 its precursors, which is only fully tested and evaluated in CESM1. The use of similar chemical
140 mechanism (MOZART) in different model versions may reduce the uncertainties in the simulation results.
141 All simulations discussed in this paper are performed at a horizontal resolution of 1.9° (latitude) and 2.5°
142 (longitude). The model has 26 vertical levels in the online configuration and 56 levels in the offline
143 configuration using specified meteorological fields; in all these cases, the model extends to
144 approximately 4 hPa (≈40 km). Offline simulations were driven by Modern Era Retrospective analysis
145 for Research and Applications, version 2 (MERRA2) meteorology (Rienecker et al., 2011). Simulations
146 using present-day emissions (2015) are labelled PD, while those using future net zero emissions (2060)
147 are labelled NZ, and these are prefixed with online or offline depending whether the model is run online

148 or driven by MERRA2 meteorology. To ensure the stability of the response to climate change, the future
 149 online simulations are run for 15 years, with the first ten years as spin-up. The CH₄ concentrations are
 150 prescribed following the SSP1-1.9 pathway using a fixed lower boundary condition. A summary of the
 151 simulations is provided in Table 1.

152

Table 1 Experimental settings

Case-name	Climate Change and Emissions		Emissions	
	online-PD	online-NZ	offline-PD	offline-NZ
Model	CESM1.2.2	CESM1.2.2	CESM2.2.0	CESM2.2.0
Component	FMOZ	FMOZ	FCSD	FCSD
Physics	CAM4	CAM4	CAM6	CAM6
Chemical mechanism	tropospheric chemistry with bulk aerosols, MOZART-4		troposphere/stratosphere chemistry with simplified VBS-SOA, MOZART-TS1	
Dynamics	Free-running	Free-running	Merra2 Nudging	Merra2 Nudging
Spin-up	2012-2014	2050-2059	2014	2014
Analyzed Year	2015-2016	2060-2064	2015	2015
Resolution	1.9°×2.5° with 26 levels	1.9°×2.5° with 26 levels	1.9°×2.5° with 56 levels	1.9°×2.5° with 56 levels
in China	2015- DPEC	2060-DPEC	2015-DPEC	2060-DPEC
Emission Outside China	2015-SSP119	2060-SSP119	2015-SSP119	2060-SSP119
CH ₄	2015-SSP119	2060-SSP119	2015-SSP119	2060-SSP119
Tagging O ₃ sources	TOAST		O ₃ S	

153

154 2.2 Emissions

155 For this analysis, we use estimates of global future anthropogenic and biomass burning emissions and
 156 future abundances of greenhouse gases and aerosols provided by the SSP1-1.9 pathway ([https://esgf-
 157 node.llnl.gov/projects/input4mips/](https://esgf-node.llnl.gov/projects/input4mips/)) along with more recent estimates for China using the Ambitious-
 158 pollution-Neutral-goals scenario from the Dynamic Projection model for Emissions in China (DPEC,
 159 <http://meicmodel.org/>). The SSP1-1.9 pathway results in a climate radiative forcing of 1.9 W m⁻² by 2100
 160 under the sustainable development path. The SSP1-1.9 pathway is a strong pollution control scenario and
 161 is the only route to limit the global average temperature increase since the preindustrial period to 1.5°C
 162 by 2100 (O'Neill et al., 2014; Rao et al., 2017; Riahi et al., 2017). The emissions inventory includes
 163 monthly O₃ precursors, aerosols, and their precursors (NO_x, CO, non-methane volatile organic (VOCs),
 164 sulfur dioxide (SO₂), ammonia (NH₃), black carbon (BC), organic carbon (OC), dimethyl sulphide
 165 (DMS)), and concentrations of greenhouse gases, such as CH₄. Biogenic emissions of VOCs are

166 calculated online in CESM using the Model of Emissions of Gases and Aerosols from Nature model
 167 (MEGAN; Guenther et al., 2006; 2012). We use emissions for the years 2015 and 2060. Over China, the
 168 anthropogenic emissions are replaced by the Ambitious-pollution-Neutral- goals scenario from DPEC
 169 (Tong et al., 2020; Cheng et al., 2021). This considers a scenario in which China achieves carbon
 170 neutrality by 2060. The DPEC anthropogenic emissions are based on SSP scenarios and MEIC, but give
 171 anthropogenic emissions at higher resolution in China which more accurately characterize China's
 172 emission sources and reflect recent rapid changes in emissions. The total anthropogenic NO emission in
 173 China in the Ambitious-pollution-Neutral- goals scenario from DPEC is 1.1 Tg yr⁻¹ lower in present day
 174 than in SSP1-1.9 and 1.5 Tg yr⁻¹ lower in 2060, but in most regions of Eastern China it is slightly higher.
 175 The combined emissions distribution for NO_x and its changes in future are shown in Figure S1. The total
 176 annual mean surface emissions of key pollutants from anthropogenic (ANT), biomass burning (BB) and
 177 biogenic (BIO) sources for the present day (2015) and future net zero (2060) over the globe and in East
 178 Asia are listed in Table 2.

179 The global anthropogenic emissions of all O₃ precursors are significantly reduced in the net zero scenario.
 180 Due to strict control policies on pollutants emissions and changes in technology and behavior, global
 181 anthropogenic NO emissions decrease from 87 Tg yr⁻¹ in present day to 19 Tg yr⁻¹ in 2060, and total
 182 anthropogenic VOCs emissions decrease from 125 Tg yr⁻¹ to 28 Tg yr⁻¹. Biomass burning emissions
 183 decrease slightly. Natural NO soil emission, VOCs biogenic emission, and CO ocean emission are
 184 assumed not to change in this study as changes in land use are relatively small. Anthropogenic emissions
 185 over East Asia account for more than 35% of the global total, with biomass combustion emissions
 186 accounting for a smaller proportion, ~10%, and natural emissions of NO, VOCs and CO accounting for
 187 ~20%. The decrease of anthropogenic emissions over East Asia (about 80% for NO) is greater than the
 188 global average, >70%, which may due to the high present day emissions over the region, especially in
 189 Eastern China. The global CH₄ concentration decreases from the current 1831 ppbv to 1312 ppbv, due
 190 to the lower global CH₄ emissions under net zero.

191 Table 2 Annual mean time-varying surface emissions of NO_x, VOCs, and CO from anthropogenic
 192 (ANT), biomass burning (BB) and biogenic (BIO) emissions for the present day (2015) and future
 193 (2060, net zero) in East Asia and over globe. Annual mean surface CH₄ mixing ratios (ppbv) are also
 194 shown.

Emission (Tg yr ⁻¹)		Globe		East Asia	
		Present Day	Net Zero	Present Day	Net Zero
NO	ANT	87.5	19.1	36.9	7.5
	BB	8.9	7.5	0.7	0.5
	Soil	10.6	10.6	2.3	2.3
	Total	106.9	37.2	39.8	10.2
VOCs	ANT	125.0	27.5	42.9	11.0

	BB	66.6	50.2	6.3	4.0
	BIO	868.5	868.5	111.0	111.0
	Total	1060.1	946.2	160.3	126.0
CO	ANT	559.8	151.7	266.9	72.7
	BB	325.5	248.2	30.2	18.9
	Ocean	20.0	20.0	1.3	1.3
	Total	905.2	419.9	298.4	92.9
CH ₄ (ppbv)		1830.5	1312.2	1860.8	1337.3

195

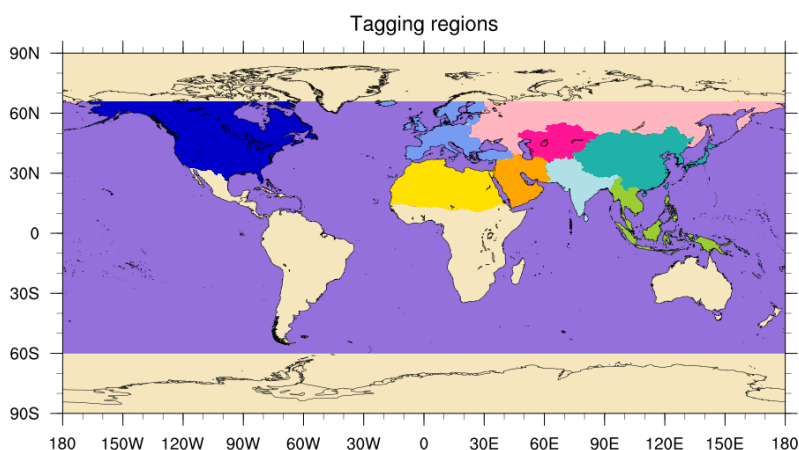
196 2.3 Tagging of ozone

197 In this study, we use the Tropospheric Ozone Attribution of Sources with Tagging (TOAST) ozone
 198 methodology in CESM1.2.2 previously described by Butler et al. (2018, 2020) to perform separate source
 199 attributions of ground-level O₃ to NO_x. The parameterizations based on the work of Butler et al. (2018,
 200 2020) include tagging the biogenic, biomass burning and anthropogenic emissions of NO_x or VOCs by
 201 their geographical source regions. This tagging methodology allows us to examine the seasonal cycle of
 202 the surface O₃ attribution in receptor regions using those defined in the Hemispheric Transport of Air
 203 Pollutants Phase 2 (HTAP2, Janssens-Maenhout et al., 2015; Koffi et al., 2016). We consider 16 sources,
 204 including 11 geographical source regions for anthropogenic NO_x emission, shown in Table 3 and Figure
 205 1, NO_x emissions from biogenic sources (BIO), biomass burning (BB), aircraft (AIR) and lightning
 206 (LIG), and O₃ originating in the stratosphere (STR).

207 Table 3 Source sector tagging of anthropogenic NO_x emissions by geographical source region, NO_x
 208 emissions from biogenic burning, soil emission, aircraft, and lightning, and the contribution of
 209 stratospheric O₃ input.

ID	Geographical region, NO _x	ID	Geographical region, NO _x	ID	Source
OCN	Oceans	NAF	Northern Africa	BIO	Biogenic NO _x
NAM	N. America	MDE	Middle East	BB	Bioburn NO _x
EUR	Europe	CAS	Central Asia	AIR	Aircraft NO _x
SAS	South Asia	SEA	South East Asia	LIG	Lightning NO _x
EAS	East Asia	RBU	Russia, Belarus, Ukraine	STR	Stratospheric O ₃
RST	Rest of World				

210



211

212 Figure 1 Geographical source regions for tagging anthropogenic NO_x emissions in this study as defined
 213 in HTAP Phase 2.

214 **2.4 Measurement Data**

215 To evaluate tropospheric column O₃ in the model simulations, we use a present-day satellite dataset of
 216 tropospheric column O₃, which was derived by combining retrievals from the Aura Ozone Monitoring
 217 Instrument (OMI) and Microwave Limb Sounder (MLS) observations ([https://acd-
 218 ext.gsfc.nasa.gov/Data_services/cloud_slice/](https://acd-ext.gsfc.nasa.gov/Data_services/cloud_slice/)). More details about the generation of this dataset are
 219 provided by Ziemke et al., (2011). The dataset resolution used in this study is 1° (Latitude) × 1.25°
 220 (Longitude) and the year is 2015. The monthly-mean thermal tropopause pressure is used to separate
 221 tropospheric and stratospheric O₃ for the model results and satellite observations.

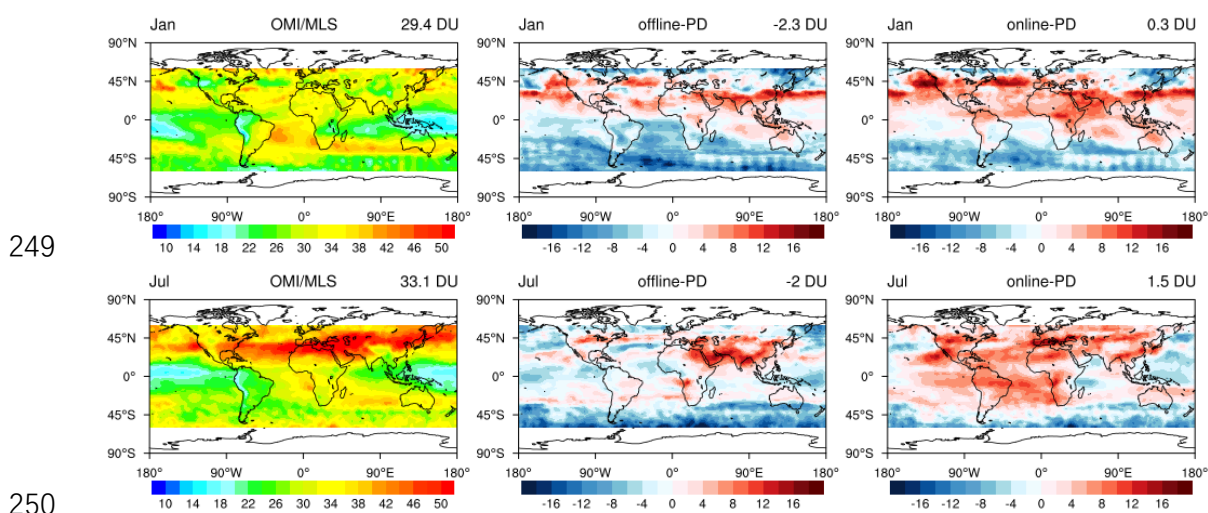
222 A High-resolution Air Quality Reanalysis Dataset over China (CAQRA, Kong, et al., 2020; Tang et al.,
 223 2020 a, b) is used to evaluate the simulated present day surface O₃ over China
 224 (<https://doi.org/10.11922/sciencedb.00053>). This dataset is generated by assimilating surface
 225 observations from the China National Environmental Monitoring Centre (CNEMC) into the Nested Air
 226 Quality Prediction Modeling System (Tang et al., 2011, Wang et al., 2000), and it provides self-consistent
 227 concentration fields of O₃ in China from 2013 to 2019 at high spatial (15 km) and temporal (1 h)
 228 resolutions. The year used in this study is 2015.

229 In addition, monthly observational surface O₃ concentration are taken from 12 regional stations of the
 230 Acid Deposition Monitoring Network in East Asia (EANET; <https://www.eanet.asia/>) for 2015: Rishiri,
 231 Ochiishi, Tappi, Sado-Seki, Happo, Oki, Yusuhara, Hedo, Mondy, Listvyanka, Kanghawa, and Chenju.
 232 The locations and altitudes of these sites are shown in Figure S2.

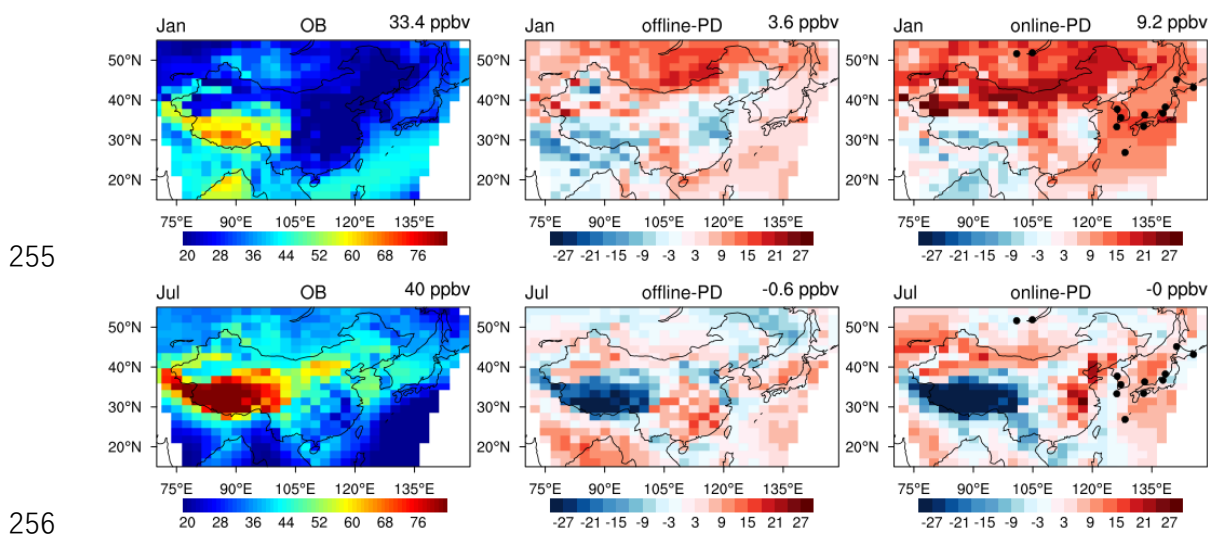
233 **3. Tropospheric ozone evaluation**

234 We compared the simulated monthly mean tropospheric column O₃ (TCO) with that derived from
 235 OMI/MLS for January and July in 2015 (Figure 2). The model captures the general features of the
 236 observed tropospheric column, reproducing the seasonal pattern, with a minimum of 15 DU at 180°E in
 237 the tropics during January and a maximum of >50 DU in northern hemisphere mid-latitudes during July.

238 The highest values in the northern mid-latitudes are overestimated in both offline and online simulations,
 239 especially during July. In the simulations, TCO was calculated by integrating the O₃ from the surface to
 240 the tropopause. Some of the differences of the simulated TCO with OMI/MLS may be due to the
 241 relatively coarse vertical resolution of the model (26 levels in online simulations and 56 levels in offline
 242 simulations). Uncertainty in the satellite dataset (exceeding 5 DU in high latitudes, Ziemke et al. 2011)
 243 might also contribute to these differences. The accuracy of the emissions inventory also affects the
 244 simulation results, especially at the surface. The global (60°S~60°N) annual mean tropospheric O₃
 245 columns from the offline and online simulations are 29.0 and 32.3 DU, respectively, which match those
 246 from OMI/MLS (31.7 DU) and the ACCMIP models mean value (30.8 DU, Young et al., 2013) well.
 247 The online simulated tropospheric ozone column on global annual average is the highest, due to the
 248 coarser vertical resolution in online simulation (Lamarque et al., 2012).



251 Figure 2 Tropospheric column O₃ (DU) from OMI/MLS (left), and the biases of offline (middle) and
 252 online (right) simulations for January and July under present day conditions. The biases are simulated
 253 result minus satellite (OML/MLS) result. The values in the right corner of each sub-figure are the
 254 average over the globe (-60°S to 60°N).



257 Figure 3 Surface O₃ mixing ratios in East Asia (ppbv) from the CAQRA reanalysis (left) and the biases
258 from offline (middle) and online (right) present day simulations in January and July. The biases are
259 simulations minus observations, and black dots show the locations of EANET observation sites. The
260 values in the right corner of each sub-figure are the regional mean for East Asia (15~55°N, 70~149°E).

261 As shown in Figure 3, surface O₃ shows substantial seasonal variations with low concentrations in winter
262 and high concentrations in summer. The spatial distributions of simulated surface O₃ concentrations
263 match the observations well. The online simulated surface O₃ (ppbv) is overestimated by 9.2 ppbv on
264 average in winter, especially in Mongolia, north and middle of China, Korea, and Japan, while the offline
265 simulation is much closer to the observation with a bias of 3.6 ppbv. The coarser resolution of the online
266 model is likely a reason for its higher bias. The comparison of simulated surface O₃ (ppbv) with EANET
267 observations show that the simulations reproduce the seasonal variations at these 12 sites (Figure S2 in
268 the Supplementary Material). In general, the performance of these simulations is very similar to those
269 from other chemical model studies (Li et al., 2019; Young et al., 2018).

270 **4 Tropospheric ozone budgets and distributions under the Net Zero scenario**

271 An overview of the global model diagnostics for the simulation experiments is given in Table 4.
272 Tropospheric O₃ burden and budget terms for present-day conditions in this study match previous results
273 well. Under net zero, the chemical production decreases from 5038 to 3392 Tg(O₃) yr⁻¹, and the chemical
274 loss decreases from 4641 to 3311 Tg(O₃) yr⁻¹. The net chemical tendency of tropospheric O₃ (NetChem
275 in Table 4) drops substantially, decreasing from the current 397 Tg(O₃) yr⁻¹ to 81 Tg(O₃) yr⁻¹, due to the
276 large reduction in O₃ precursor emissions (Table 2). This results in an increase in the lifetime of
277 tropospheric O₃ from 20 days to 22 days. The residual term, which principally reflects net transport from
278 the stratosphere, increases from the current 595 to 626 Tg(O₃) yr⁻¹. The global tropospheric O₃ burden
279 decreases by about 20%, from 316 Tg to 247 Tg, bringing it close to the mean burden of 239±22 Tg
280 estimated for the pre-industrial period (Young et al., 2013, Griffiths et al., 2021). The burden of O₃ of
281 stratospheric origin in the troposphere (O₃S) increases from 69 Tg to 77 Tg. This increased stratospheric
282 contribution may be due to the enhancement of stratospheric circulation and increased stratosphere-
283 troposphere exchange caused by climate change (Sudo et al., 2003; Lu et al., 2019), and has been seen
284 in previous studies (e.g., Zanis et al., 2022). In addition, the longer chemical lifetime allows stratospheric
285 O₃ to persist for longer in the troposphere, enhancing the stratospheric contribution. Compared with pre-
286 industrial conditions (Griffiths et al., 2021; Table 4), the net chemical production rate is slower, while
287 the stratospheric contribution is higher. This may indicate that anthropogenic influence is somewhat
288 weaker than that in the pre-industrial. Compared with other SSP scenarios, particularly the much-studied
289 SSP3-7.0 pathway (Liu et al., 2022; Griffiths et al., 2021), SSP1-1.9 provides a more positive perspective
290 on the opportunities for controlling future tropospheric O₃, and the benefits for air quality.

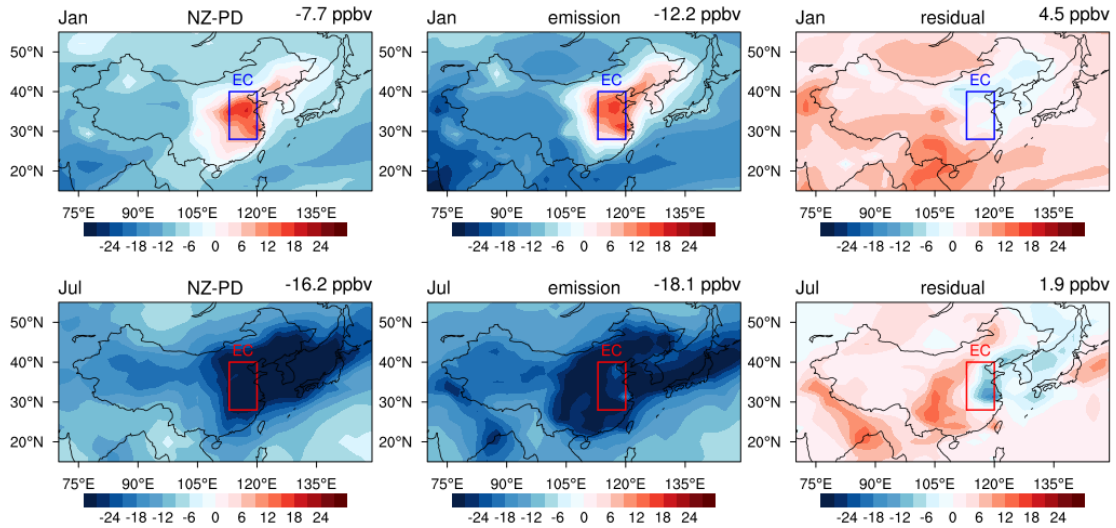
291 Over East Asia, the net photochemical production of tropospheric O₃ also decreases significantly, from
292 the current 227 Tg(O₃) yr⁻¹ to 137 Tg(O₃) yr⁻¹ under net zero, but the reduction is less than the global
293 average and this is attributed to the higher emissions and smaller reductions in precursors over East Asia.
294 The negative “Residual” budget term for East Asia indicates that the production is larger than the sink,

295 and the total contribution of vertical and horizontal transport from outside of East Asia is negative. This
 296 indicates that there is net outflow from East Asia with transport of tropospheric O₃ to other regions, and
 297 this outflow is weakened in the future, from 89 Tg(O₃) yr⁻¹ under present day conditions to 38 Tg(O₃) yr⁻¹
 298 ¹ under net zero. The tropospheric O₃ burden in East Asia decreases from 25 Tg to 19 Tg, while the
 299 burden of O₃ from the stratosphere increases slightly from 5 Tg to 6 Tg. The tropospheric O₃ lifetime in
 300 East Asia is 15 days, slightly lower than the global average due to the faster photochemical processing
 301 under relatively high anthropogenic emissions. But the increase of ~2 days matches that of the global
 302 average.

303 Table 4 Global tropospheric O₃ burden (Tg) and budget terms (Tg yr⁻¹) in chemical transport models.

Models	Prod	Loss	NetChem	Residual	DryDep	Burden (O ₃ /O ₃ S)	Lifetime (days)	Reference
Globe				STE				
33	3948±761	3745±554	245±346	636±273	902±255	307±38	21-25	Wild (2007)
17	4465±514	4114±409	396±247	529±105	949±222	314±33	22±2	Stevenson et al. (2006)
15	5110±606	4668±727	442±309	552±168	1003±200	344±39	22±2	Young et al. (2013)
PI	2549	2437	112	415	528	241	29	Griffiths et
PD	4510	3948	562	284	846	337	26	al. (2021)
PD	5038	4641	397	595	992	316/69	20	This study
NZ	3392	3311	81	626	707	247/77	22	This study
East Asia				Transport				
PD	682	455	227	-89	138	25/5	15	This study
NZ	430	293	137	-38	99	19/6	17	This study

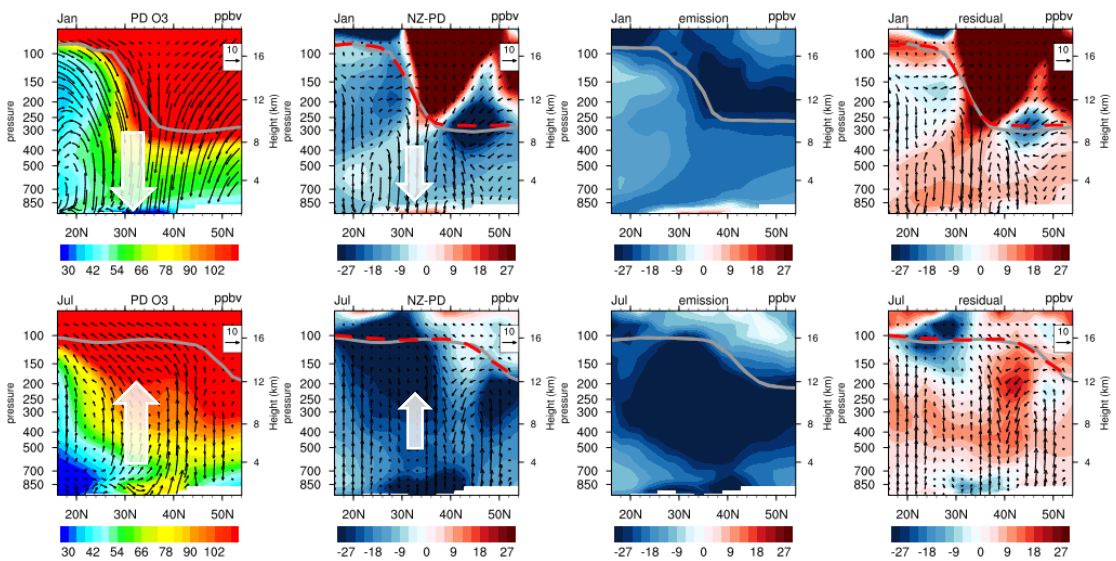
304 Prod for chemical production, Loss for chemical loss, Prod-Loss for net chemical production (NetChem)
 305 and DryDep for dry deposition; Residual is the term balance by Residual=Loss-Prod+DryDep. Units of
 306 Prod, Loss, NetChem, Residual and DryDep are in Tg(O₃) yr⁻¹, Burden in Tg(O₃), and Lifetime in days.
 307 The climatological pressure tropopause is used. PD is the online present day experiment simulation. NZ
 308 is online net zero experiment simulation. The results of Griffiths et al. (2021) are the average of four
 309 models (UKESM1, CESM2-WACCM, GFDL-ESM4, MRI-ESM2-0), and PD is the average from 1995
 310 to 2004, while PI (pre-industrial) is the average from 1850 to 1859.



311

312

313 Figure 4 Changes in surface O_3 mixing ratio (ppbv) over China in January and July between present
 314 day and net zero (online-NZ minus online-PD, left), and changes due to emissions (offline-NZ minus
 315 offline-PD, middle) and the residual (left minus middle panel, right). The values in the right corner of
 316 each panel are the regions mean over East Asia ($15^{\circ}\sim 55^{\circ}N$, $70^{\circ}\sim 149^{\circ}E$). The frame is the region of
 317 Eastern China (EC, $28^{\circ}\sim 40^{\circ}N$, $113^{\circ}\sim 120^{\circ}E$).



318

319

320 Figure 5 Zonal mean O_3 cross section (ppbv) and wind speed (vectors, $v: m s^{-1}$, $w: (-500) pa s^{-1}$) over
 321 Eastern China (longitudes $111\sim 122^{\circ}E$) in January and July under present day (online-PD, left), the
 322 changes in O_3 and wind speed (second panels) and changes due to emissions (third panels) and the
 323 residual (second panels minus third panels, right). Grey lines show the tropopause location under
 324 present day conditions; the red dashed lines show the tropopause location under net zero.

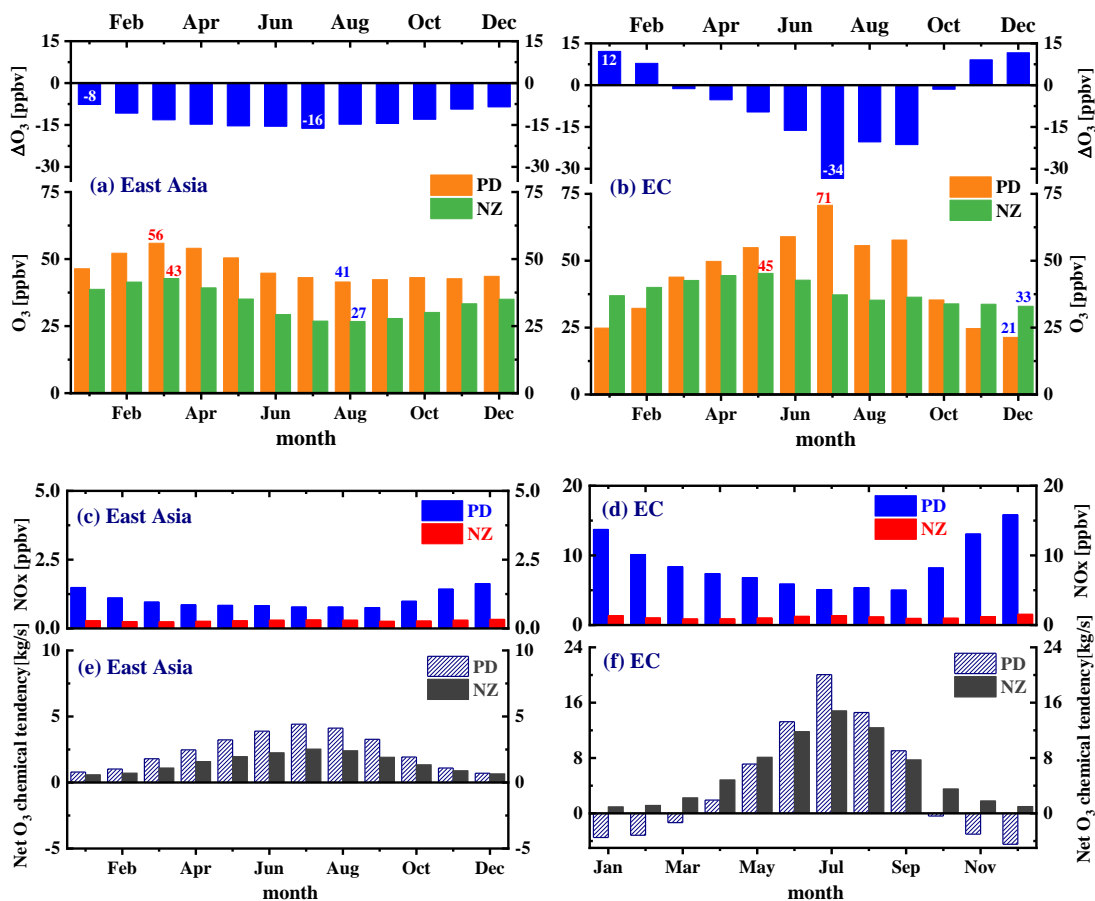
325 The changes in surface O_3 over East Asia between 2015 and 2060 in winter and summer are shown in
 326 Figure 4. The left panels show the changes in surface O_3 under net zero (online-NZ minus online-PD),
 327 which include the effects of climate change and emissions changes. The climate change in this study

328 includes changes in atmospheric parameters (air temperature, relative humidity, atmospheric circulation
329 etc.) from the free-run of atmospheric simulation experiments (online). The climate change along SSP119
330 is much weaker than other pathways, and the change in global surface air temperature in this study is not
331 significant (Figure S3 in Supplementary Material). Over East Asia, the surface air temperature is
332 increased by an annual average of 0.2°C. The middle panels show the changes in surface O₃ under the
333 effect of emissions changes only (offline-NZ minus offline-PD). The right panels show the residual
334 changes in surface O₃ which reflect the effect of climate change, but are also influenced by differences
335 in model setup between the online and offline simulations (left panels minus middle panels). Surface O₃
336 decreases in East Asia under net zero, with a mean reduction of 7.7 ppbv in winter and a greater reduction
337 of 16.2 ppbv in summer. Turnock et al. (2019) estimated an annual mean reduction of 8 ppbv in 2050
338 along the SSP1-1.9 pathway, slightly less than we find here. However, we have used the more stringent
339 DPEC Ambitious-pollution-Neutral-goals emission scenario for China rather than the standard SSP1-1.9
340 pathway and we note that anthropogenic NO emissions in China are 1.5 Tg (NO) yr⁻¹ lower in this
341 scenario than those in SSP1-1.9. Surface O₃ over Eastern China and South Korea increases in winter in
342 these scenarios, driven by the reduction in emissions (left and middle panels). This increase in surface
343 O₃ is caused by a weakening of titration under lower regional NO emissions in the future. The influence
344 of climate change on surface O₃ is relatively weak, and leads to an increase of surface O₃ in most parts
345 of East Asia (right panels). This is partly due to enhanced vertical circulation leading to an increased
346 contribution from stratospheric O₃ (Akritidis et al., 2019; shown in Figure S4) and the photochemical
347 change under warmer climate (Zanis et al., 2022). Xu et al. (2022) also showed that emission reduction
348 is far more effective than climate change in improving air quality (PM_{2.5} and O₃) over East Asia under a
349 carbon neutral reduction pathway. Here we will use tagging simulations to quantify the contributions of
350 different sources to surface O₃ changes over East Asia, especially over Eastern China where surface O₃
351 increases in winter and decreases in summer.

352 It can be seen from the vertical distribution of O₃ and circulation (shown in the first panels of Figure 5)
353 that the O₃ concentration increases with altitude under present day conditions. At the same altitude, the
354 O₃ concentration is higher in middle and high latitudes than in low latitude. In winter, there is strong net
355 descent of air over eastern China (30~40°N), which weakens in spring, and turns to updraft in summer.
356 These may be due to the weakened Brewer-Dobson circulation and strengthened convection (Butchart,
357 2014; Wild and Akimoto, 2001). As shown in the second panels of Figure 5, there is a net decrease in
358 tropospheric O₃ in future, with an increase only seen near 30°N very close to the surface. In summer, the
359 reduction in tropospheric O₃ is greatest, especially near the tropopause where it exceeds 30 ppbv. In
360 addition, due to the temperature increase and circulation enhancement in the future, the tropopause height
361 increases, especially in the mid-latitude region in winter where the increase is about 7 hPa. As seen from
362 the third panels of Figure 5, the reduction of emissions from aircraft (NO emissions in Figure S1) leads
363 to a reduction in O₃ production, and the O₃ concentration near the tropopause decreases substantially in
364 the future. However, other factors such as climate change (the fourth panels in Figure 5) lead to increases
365 in tropospheric O₃ by 2060.

366 **5 The contribution of O₃ chemistry and intercontinental transport**

367 Surface O₃ shows substantial seasonal variation over East Asia with a peak in spring, as shown in Figure
368 6a. It reaches a maximum (56 ppbv) in March and is lowest (41 ppbv) in August under present day
369 conditions. Under net zero, the concentration of surface O₃ is lower throughout the year, and while the
370 peak is still in March, the mixing ratio drops to 43 ppbv. The decrease is greatest in July, 16 ppbv, which
371 reflects weaker chemical production in summertime under lower future emissions (Figure 6e). In contrast,
372 surface O₃ over Eastern China is highest (71 ppbv) in July and lowest (21 ppbv) in December under
373 present day conditions (Figure 6b). Under net zero, surface O₃ increases in winter and decreases in
374 summer, and the peak shifts from July to May, due to the changes in O₃ precursors emissions (Bowman
375 et al., 2021). This shifts the seasonal peak from summer towards spring, when it is more greatly
376 influenced by stratosphere-troposphere exchange. The decrease is highest in July, as seen over the wider
377 East Asian region, but is twice as large, at 34 ppbv, reflecting the stronger present-day emissions over
378 Eastern China. There is a substantial increase in O₃ in January of 12 ppbv, reflecting reduced titration by
379 NO. The concentration of surface NO_x decreases more than 60%, and by an even larger factor in winter
380 (~90%, 14 ppbv); and its seasonal variation is reduced which accounts for the reduction in anthropogenic
381 emissions (Figure 6d). In terms of the O₃ chemical budget, local chemical production and destruction are
382 both reduced in the future. The peak in net O₃ chemical production still occurs in summer which
383 highlights that photochemical processes continue to dominate the seasonal variation of surface O₃ in
384 Eastern China in future (Figure 6f). However, the net chemical destruction that currently occurs in winter
385 is replaced with a small net O₃ production, reflecting the reduced titration of O₃ by NO under future
386 emissions, which are very greatly reduced under net zero (Liu et al., 2022, 2023).



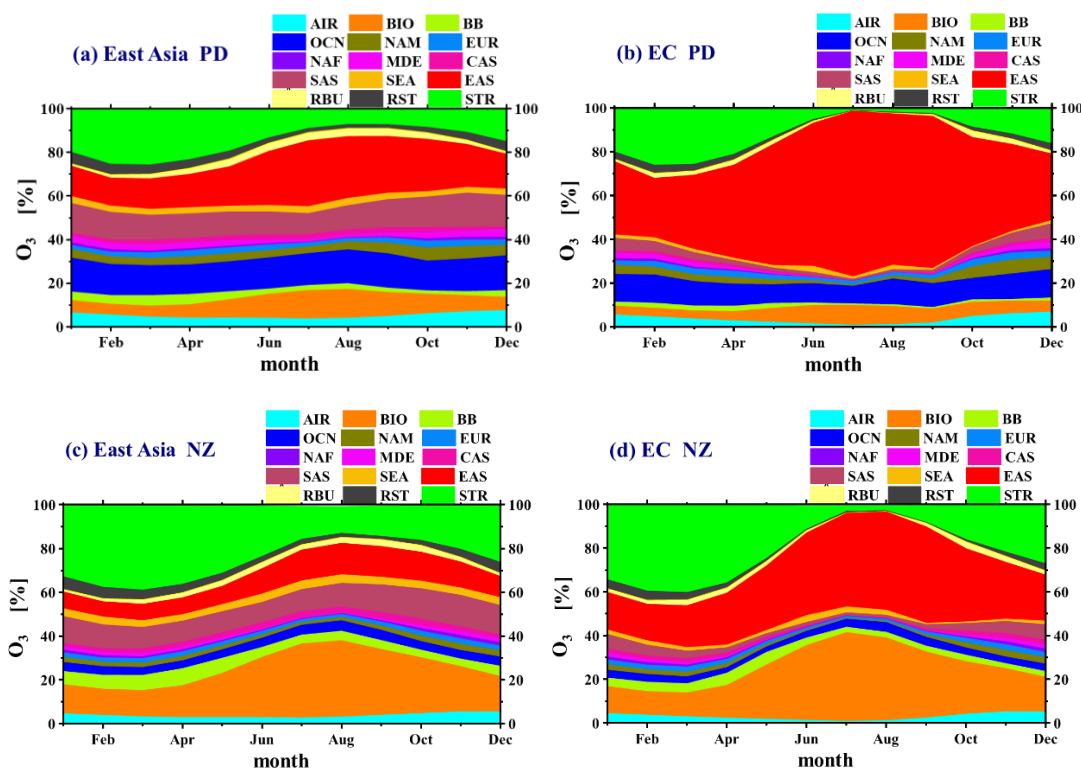
387

388

389 Figure 6 Comparison of O₃ (a, b), NO_x (c, d) and net O₃ chemical tendency (e, f) at the surface under
 390 present day and net zero conditions over East Asia (left) and Eastern China (right). Results are from the
 391 online simulations (online-PD and online-NZ). Maximum and minimum O₃ mixing ratios are
 392 highlighted in red and blue, respectively, and the largest and smallest O₃ changes are indicated in
 393 white. The net O₃ chemical tendency is the net photochemical production rate of O₃ (kg/s).

394 We quantify the contributions of regional transport and stratospheric input to surface O₃ on a monthly
 395 basis in Figure 7. In present day (Figure 7a), we find that the contribution of anthropogenic NO emissions
 396 from East Asia (EAS) is highest, especially in summer when it reaches 30% (12 ppbv in Figure 8). The
 397 total contributions from anthropogenic NO emissions outside East Asia (EAS_out, without ocean) is 33%
 398 (16 ppbv) on average with little seasonal variation, and it is highest over South Asia (SAS), accounting
 399 for 12% (6 ppbv). The contribution from biogenic NO emissions from soils (BIO) is also important,
 400 exceeding 10% (5 ppbv in Figure 8) in summer. The contributions from the ocean (OCN) show little
 401 seasonal variation, contributing 15% (6 ppbv). Under net zero (Figure 7c), the anthropogenic contribution
 402 from East Asia drops dramatically, to 14% (4 ppbv in Figure 8) in summer, due to the reduced emissions
 403 of O₃ precursors. The total contributions from anthropogenic NO emissions outside East Asia decrease
 404 to 28% (10 ppbv) on average, 7 ppbv in summer (in Figure 8). The contribution of biogenic sources is
 405 enhanced, and forms the dominant contributor to surface O₃ under net zero, especially in summer, ~40%
 406 (9 ppbv in Figure 8). The emissions from biogenic sources do not vary from year to year in this study.
 407 The enhanced contribution of biogenic sources is mainly due to the increased O₃ production efficiency,

408 which is a consequence of lower O₃ precursor concentrations (Kleinman et al., 2002; Zaveri et al., 2003).
 409 The contribution of oceanic sources decreases to 4% (1 ppbv) due to reduced emissions from shipping.
 410 The contribution from stratospheric O₃ (STR) is highest in March (26%, 14 ppbv), and lowest in August
 411 (7%, 3 ppbv) under present day conditions. Under net zero, the highest contribution is increased to 39%
 412 (17 ppbv), and the lowest contribution is also increased, to 12% (3 ppbv). This may be due to enhanced
 413 stratospheric circulation, slower photochemical loss and a longer lifetime of O₃ in the troposphere
 414 allowing greater transport of stratospheric O₃ to the ground.



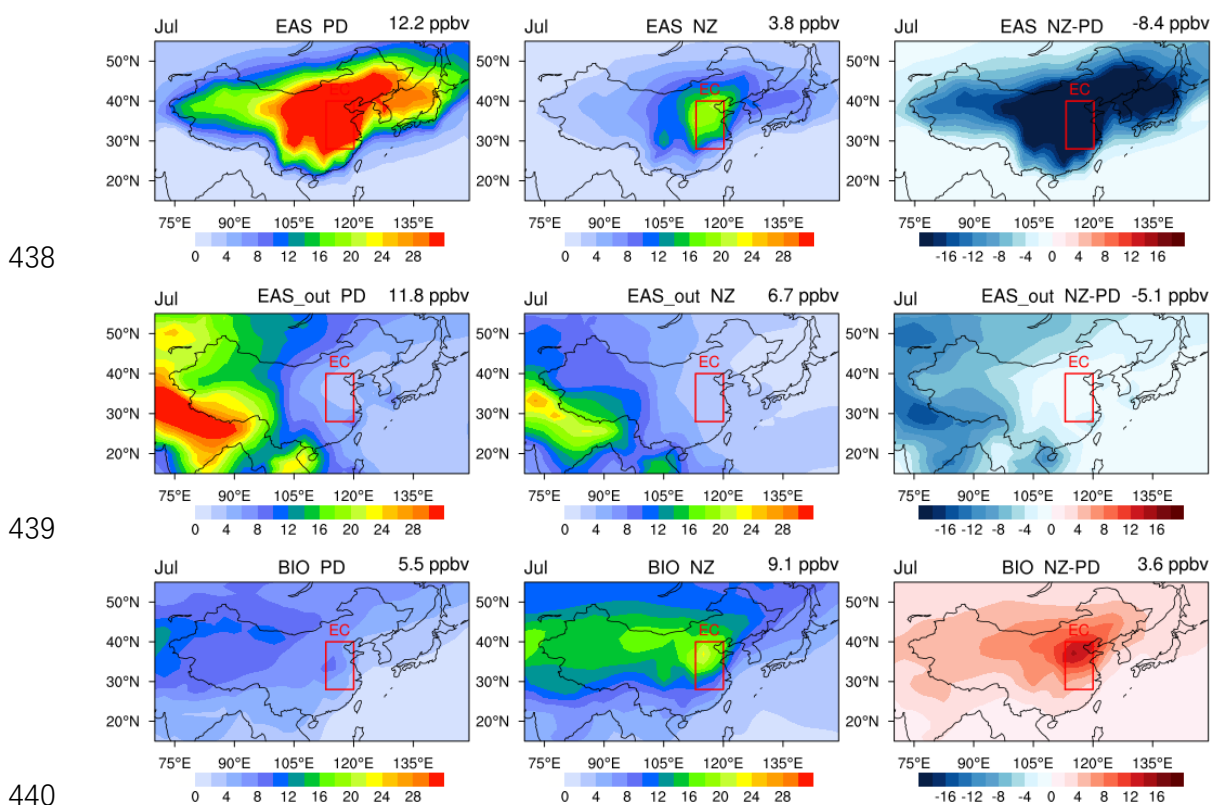
415

416

417 Figure 7 Contributions of different sources to surface O₃ under present day and net zero conditions over
 418 East Asia (a, c) and Eastern China (b, d). Results are from the online simulations (online-PD and
 419 online-NZ). 11 geographical source regions are used for anthropogenic NO_x emission. BIO, BB, AIR,
 420 and LIG are the contribution of NO_x emission from biogenic sources, biomass burning, aircraft and
 421 lightning to O₃. STR is the contribution of O₃ originating in the stratosphere.

422 Over Eastern China (Figure 7b), the contribution from East Asian anthropogenic sources is highest,
 423 especially in summer when it exceeds 70% (43 ppbv, shown in Figure 8). The total contributions from
 424 anthropogenic NO emissions out of East Asia is 16 % (6 ppbv) on average, 4 ppbv in summer (in Figure
 425 8). Biogenic and oceanic sources make a smaller contribution over this region, only 6% (3 ppbv) and 10%
 426 (5 ppbv) on average, respectively. Under net zero (Figure 7d), the contribution of East Asian
 427 anthropogenic sources drops to 42% (16 ppbv) in summer, but remains the dominant source of surface
 428 O₃ in Eastern China. The total contributions from anthropogenic NO emissions outside East Asia show
 429 little change. The contribution of biogenic sources is enhanced, especially in summer, reaching 40% (14
 430 ppbv in Figure 8), close to the contribution from East Asian sources. The stratospheric contribution is

431 highest in early spring (25%, 11 ppbv), and lowest in summer (2%, 1 ppbv). Under net zero, the
 432 stratospheric contribution is enhanced to 40% (17 ppbv) in March and 3% (1 ppbv) in summer, similar
 433 to the seasonal contributions over East Asia. In addition, the high NO concentration in heavily urbanized
 434 Eastern China has a titration effect on O₃, but the strong future decreases in NO weaken this effect,
 435 reducing the loss of stratospheric O₃ as well as O₃ from local sources. Overall, surface O₃ shows
 436 substantial decreases through much of the year, and the local contribution is reduced, which highlights
 437 the beneficial role that net zero policies may have for controlling surface O₃ pollution in China.



441 Figure 8 The contributions of anthropogenic NO emissions over East Asia (EAS, first row), outside
 442 East Asia (EAS_out, second row), and biogenic emission (BIO, third row) on surface O₃ (ppbv) over
 443 East Asia in July of present day (online-PD, left) and net zero (online-NZ, middle), and the differences
 444 between PD and NZ (online-NZ minus online-PD, right). The values in the right corner of each sub-
 445 figure are the regional mean over East Asia. The box shows the region of Eastern China.

446 6 Summary and conclusions

447 We quantify tropospheric O₃ budgets, spatiotemporal distributions of future surface O₃ in East Asia and
 448 regional O₃ source contributions for 2060 under a net zero scenario, using the NCAR Community Earth
 449 System Model (CESM) and online O₃ tagging methods. The simulated monthly mean global tropospheric
 450 column O₃ and surface O₃ mixing ratios over East Asia capture the general features in observations well
 451 under present day conditions. The offline simulations perform better than online simulations, as the
 452 nudging provides a closer match to observed meteorological conditions. The tropospheric O₃ burden and

453 budget terms under present-day conditions in this study also matches those of previous model studies
454 well.

455 The simulated tropospheric O₃ burden is likely to decrease from 316 Tg under present day conditions to
456 247 Tg by 2060 under the net zero scenario. This brings it close to that found in previous studies under
457 preindustrial conditions of 239±22 Tg (Young et al., 2013). Future tropospheric O₃ chemical production
458 and loss are both reduced, and the net chemical tendency decreases from 397 to 81 Tg(O₃) yr⁻¹. The
459 contribution of stratospheric O₃ increases from 69 to 77 Tg, due to enhancement of atmospheric
460 circulation and increased stratosphere-troposphere exchange caused by climate change and the longer
461 chemical lifetime of stratospheric O₃ in the troposphere under decreased anthropogenic emissions of
462 pollutants. The mean tropospheric lifetime of O₃ is increased by 2 days, ~10%. Over East Asia, one of
463 the highest anthropogenic emissions regions, the O₃ burden decreases from 25 to 19 Tg, and the net
464 chemical tendency drops from 227 to 137 Tg(O₃) yr⁻¹. East Asia is a region of net O₃ production, and the
465 outflow is expected to decrease from 89 to 38 Tg(O₃) yr⁻¹. The burden of O₃ from the stratosphere
466 increases from 5 to 6 Tg. The lifetime of tropospheric O₃ over East Asia is shorter than the global average,
467 ~15 days, due to the high anthropogenic emissions, but increases by 2 days, similar to the global mean.
468 Compared with other SSP scenarios, particularly the much-studied SSP3-7.0 pathway, SSP1-1.9 provides
469 a more positive perspective on the opportunities for controlling future tropospheric O₃, and the benefits
470 for the improvement of air quality.

471 Regional average surface O₃ decreases throughout the year over East Asia, with highest decreases in
472 summer (16 ppbv) in the future under the net zero scenario. Over Eastern China, the peak in surface O₃
473 shifts from July to May. Surface O₃ decreases strongly in July (34 ppbv), and increases in winter,
474 especially in January, 12 ppbv. The increased O₃ in winter is caused by reduced titration of O₃ by NO
475 associated with lower anthropogenic NO emissions, and enhanced stratospheric input. The tropospheric
476 O₃ over most regions decreases due to the large decrease in O₃ precursors emissions. Climate change
477 leads to only a small increase in tropospheric O₃ under this scenario. Local anthropogenic emissions play
478 a dominant role in controlling O₃ changes over East Asia in summer, but this will drop substantially from
479 30% in present day to 14% under net zero. The contribution of biogenic sources is enhanced, and forms
480 the dominant contributor to future surface O₃, especially in summer, ~40%. This enhanced contribution
481 of biogenic sources is due here to increased O₃ production efficiency associated with reduced O₃
482 precursors concentrations, but may be underestimated if biogenic emissions also increase in future as
483 expected. The lower extent of climate change along SSP119 leads to relatively little impact on
484 tropospheric O₃ under net zero, while the emission reductions associated with net zero policies are
485 sufficient to mitigate surface O₃ pollution over East Asia, especially in summer.

486 The combined emissions and O₃ tagging method used here provide a reliable way to quantify the changes
487 of tropospheric O₃ and its sources in future under a net zero scenario. The results of this study clarify the
488 separate impacts of climate change and emissions on tropospheric O₃ changes over East Asia, and
489 highlight the significance of controlling O₃ precursors emissions along the net zero scenario, especially

490 anthropogenic emissions. The reduction of anthropogenic O₃ precursors emission should be the most
491 effective way to control the increase of tropospheric O₃, which requires joint efforts on a global scale.

492

493 **Competing interests**

494 The authors declare that they have no conflict of interest.

495 **Acknowledgements**

496 This study was supported by the National Key Research and Development Program of China (Grant No.,
497 2022YFC3701204), the National Natural Science Foundation of China (Grant No., 42021004), and Key
498 Laboratory of Atmospheric Chemistry, China Meteorological Administration (LAC/CMA, Grant No.,
499 2023B05). Numerical calculations in this paper have been performed on the high-performance computing
500 system at the High Performance Computing Center, Nanjing University of Information Science and
501 Technology. The authors would like to thank Prof. Tim Butler and Dr. Aurelia Lupascu at the Institute
502 for Advanced Sustainability Studies (now the Research Institute for Sustainability) in Potsdam, Germany
503 for helping us to update the TOAST source attribution code in the CESM model.

504 **Data availability**

505 CAQRA can be freely downloaded at <https://doi.org/10.11922/sciencedb.00053>, and the prototype
506 product, which contains the monthly and annual means of the CAQRA dataset, is available at
507 <https://doi.org/10.11922/sciencedb.00092>. The simulated O₃ data generated in this study are available on
508 <https://doi.org/10.5281/zenodo.8137796>.

509

510 **References:**

511 Akritidis, D., Pozzer, A., and Zanis, P.: On the impact of future climate change on tropopause folds and
512 tropospheric ozone, *Atmos. Chem. Phys.*, 19, 14387–14401, [https://doi.org/10.5194/acp-19-14387-](https://doi.org/10.5194/acp-19-14387-2019)
513 2019, 2019.

514 Allen, R. J., Turnock, S., Nabat, P., Neubauer, D., Lohmann, U., Olivie, D., Oshima, N., Michou, M.,
515 Wu, T., Zhang, J., Takemura, T., Schulz, M., Tsigaridis, K., Bauer, S. E., Emmons, L., Horowitz, L.,
516 Naik, V., van Noije, T., Bergman, T., Lamarque, J.-F., Zanis, P., Tegen, I., Westervelt, D. M., Le
517 Sager, P., Good, P., Shim, S., O'Connor, F., Akritidis, D., Georgoulias, A. K., Deushi, M., Sentman,
518 L. T., John, J. G., Fujimori, S., and Collins, W. J.: Climate and air quality impacts due to mitigation
519 of non-methane near-term climate forcers, *Atmos. Chem. Phys.*, 20, 9641–9663,
520 <https://doi.org/10.5194/acp-20-9641-2020>, 2020.

521 Bowman, H., Turnock, S., Bauer, S. E., Tsigaridis, K., Deushi, M., Oshima, N., O'Connor, F. M.,
522 Horowitz, L., Wu, T., Zhang, J., Kubistin, D., and Parrish, D. D.: Changes in anthropogenic precursor

523 emissions drive shifts in the ozone seasonal cycle throughout the northern midlatitude troposphere,
524 *Atmos. Chem. Phys.*, 22, 3507–3524, <https://doi.org/10.5194/acp-22-3507-2022>, 2022.

525 Butchart, N.: The Brewer-Dobson circulation, *Reviews of Geophysics*, 52(2), 157-184,
526 <https://doi.org/10.1002/2013RG000448>, 2014.

527 Butchart, N., Charlton-Perez, A. J., Cionni, I., Hardiman, S. C., Haynes, P. H., Kruger, K., Kushner, P.
528 J., Newman, P. A., Osprey, S. M., Perlwitz, J., Sigmond, M., Wang, L., Akiyoshi, H., Austin, J.,
529 Bekki, S., Baumgaertner, A., Braesicke, P., Bruhl, C., Chipperfield, M., Dameris, M., Dhomse, S.,
530 Eyring, V., Garcia, R., Garny, H., Jockel, P., Lamarque, J.-F., Marchand, M., Michou, M.,
531 Morgenstern, O., Nakamura, T., Pawson, S., Plummer, D., Pyle, J., Rozanov, E., Scinocca, J.,
532 Shepherd, T. G., Shibata, K., Smale, D., Teyssedre, H., Tian, W., Waugh, D. and Yamashita, Y.:
533 Multi-model climate and variability of the stratosphere, *J. Geophys. Res.*, 116, D05102,
534 <https://doi.org/10.1029/2010JD014995>, 2011.

535 Butler, T., Lupascu, A., Coates, J., and Zhu, S.: TOAST 1.0: Tropospheric Ozone Attribution of Sources
536 with Tagging for CESM 1.2.2, *Geosci. Model Dev.*, 11, 2825–2840, [https://doi.org/10.5194/gmd-11-](https://doi.org/10.5194/gmd-11-2825-2018)
537 [2825-2018](https://doi.org/10.5194/gmd-11-2825-2018), 2018.

538 Butler, T., Lupascu, A. and Nalam A.: Attribution of ground-level ozone to anthropogenic and natural
539 sources of nitrogen oxides and reactive carbon in a global chemical transport model, *Atmos. Chem.*
540 *Phys.*, 20, 10707–10731, <https://doi.org/10.5194/acp-20-10707-2020>, 2020.

541 Cheng, J., Tong, D., Zhang, Q., Liu, Y., Lei, Y., Yan, G., Yan, L., Yu, S., Cui, R. Y., Clarke, L., Geng,
542 G. N., Zheng, B., Zhang, X, Y., Davis, J. S., and He, K. B.: Pathways of China’s PM_{2.5} air quality
543 2015–2060 in the context of carbon neutrality, *Natl. Sci. Rev.*, nwab078,
544 <https://doi.org/10.1093/nsr/nwab078>, 2021.

545 Cionni, I., Eyring, V., Lamarque, J.F., Randel, W.J., Stevenson, D.S., Wu, F., Bodeker, G.E., Shepherd,
546 T.G., Shindell, D.T., Waugh, D.W.: Ozone database in support of CMIP5 simulations: results and
547 corresponding radiative forcing, *Atmos. Chem. Phys.*, 11, 11267–11292. [https://doi.org/10.5194/acp-](https://doi.org/10.5194/acp-11-11267-2011)
548 [11-11267-2011](https://doi.org/10.5194/acp-11-11267-2011), 2011.

549 Danabasoglu, G., Lamarque, J. -F., Bacmeister, J., Bailey, D. A., DuVivier, A. K., Edwards, J., Emmons,
550 L. K., Fasullo, J., Garcia, R., Gettelman, A., Hannay, C., Holland, M. M., Large, W. G., Lauritzen, P.
551 H., Lawrence, D. M., Lenaerts, J. T. M., Lindsay, K., Lipscomb, W. H., Mills, M. J., Neale, R., Oleson,
552 K. W., Otto-Bliesner, B., Phillips, A. S., Sacks, W., Tilmes, S., Kampenhout, L. van, Vertenstein, M.,
553 Bertini, A., Dennis, J., Deser, C., Fischer, C., Fox-Kemper, B., Kay, J. E., Kinnison, D., Kushner, P.
554 J., Larson, V. E., Long, M. C., Mickelson, S., Moore, J. K., Nienhouse, E., Polvani, L., Rasch, P. J.,
555 Strand, W. G.: The Community Earth System Model Version 2 (CESM2), *J. Adv. Model. Earth Syst.*,
556 12(2). <https://doi.org/10.1029/2019MS001916>, 2020.

557 Emberson, L.: Effects of ozone on agriculture, forests and grasslands, *Philosophical Transactions of The*
558 *Royal Society A Mathematical Physical and Engineering Sciences*, 378(2183), 20190327,
559 <https://doi.org/10.1098/rsta.2019.0327>, 2020.

560 Emmons, L. K., Walters, S., Hess, P. G., Lamarque, J.-F., Pfister, G. G., Fillmore, D., Granier, C.,
561 Guenther, A., Kinnison, D., Laepple, T., Orlando, J., Tie, X., Tyndall, G., Wiedinmyer, C., Baughcum,
562 S. L., and Kloster, S.: Description and evaluation of the Model for Ozone and Related chemical
563 Tracers, version 4 (MOZART-4), *Geosci. Model Dev.*, 3, 43–67, [https://doi.org/10.5194/gmd-3-43-](https://doi.org/10.5194/gmd-3-43-2010)
564 2010, 2010.

565 Eyring, V., Bony, S., Meehl, G. A., Senior, C. A., Stevens, B., Stouffer, R. J., and Taylor, K. E.: Overview
566 of the Coupled Model Intercomparison Project Phase 6 (CMIP6) experimental design and
567 organization, *Geosci. Model Dev.*, 9, 1937–1958, <https://doi.org/10.5194/gmd-9-1937-2016>, 2016.

568 Fan, X., Duan, Q., Shen, C., Wu, Y., and Xing, C.: Global surface air temperatures in CMIP6: historical
569 performance and future changes, *Environ. Res. Lett.*, 15, 104056, [https://doi.org/10.1088/1748-](https://doi.org/10.1088/1748-9326/abb051)
570 9326/abb051, 2020.

571 Griffiths, P. T., Murray, L. T., Zeng, G., Shin, Y. M., Abraham, N. L., Archibald, A. T., Deushi, M.,
572 Emmons, L. K., Galbally, I. E., Hassler, B., Horowitz, L. W., Keeble, J., Liu, J., Moeni, O., Naik,
573 V., O'Connor, F. M., Oshima, N., Tarasick, D., Tilmes, S., Turnock, S. T., Wild, O., Young, P. J.,
574 and Zanis, P.: Tropospheric ozone in CMIP6 simulations, *Atmos. Chem. Phys.*, 21, 4187–4218,
575 <https://doi.org/10.5194/acp-21-4187-2021>, 2021.

576 Guenther, A. B., Jiang, X., Heald, C. L., Sakulyanontvittaya, T., Duhl, T., Emmons, L. K., and Wang,
577 X.: The Model of Emissions of Gases and Aerosols from Nature version 2.1 (MEGAN2.1): An
578 extended and updated framework for modeling biogenic emissions, *Geosci. Model Dev.*, 5(6), 1471–
579 1492, <https://doi.org/10.5194/gmd-5-1471-2012>, 2012.

580 Guenther, A., Karl, T., Harley, P., Wiedinmyer, C., Palmer, P. I., and Geron, C.: Estimates of global
581 terrestrial isoprene emissions using MEGAN (Model of Emissions of Gases and Aerosols from
582 Nature), *Atmos. Chem. Phys.*, 6, 3181–3210, <https://doi.org/10.5194/acp-6-3181-2006>, 2006.

583 Heald, C. L., Henze, D. K., Horowitz, L. W., Feddema, J., Lamarque, J.-F., Guenther, A., Hess, P. G.,
584 Vitt, F., Seinfeld, J. H., Goldstein, A. H., and Fung, I.: Predicted change in global secondary organic
585 aerosol concentrations in response to future climate, emissions, and land use change, *J. Geophys.*
586 *Res.-Atmos.*, 113, D05211, <https://doi.org/10.1029/2007JD009092>, 2008.

587 Hong, C. P., Zhang, Q., Zhang, Y., Davis, S. J., Tong, D., Zheng, Y. X., Liu, Z., Guan, D., He, K. B.,
588 Schellnhuber, H. J.: Impacts of climate change on future air quality and human health in China, *Proc*
589 *Natl Acad Sci*, 116(35), 17193–17200, <https://doi.org/10.1073/pnas.1812881116>, 2019.

590 Janssens-Maenhout, G., Crippa, M., Guizzardi, D., Dentener, F., Muntean, M., Pouliot, G., Keating, T.,
591 Zhang, Q., Kurokawa, J., Wankmüller, R., Denier van der Gon, H., Kuenen, J. J. P., Klimont, Z.,

592 Frost, G., Darras, S., Koffi, B., and Li, M.: HTAP_v2.2: a mosaic of regional and global emission
593 grid maps for 2008 and 2010 to study hemispheric transport of air pollution, *Atmos. Chem. Phys.*, 15,
594 11411–11432, <https://doi.org/10.5194/acp-15-11411-2015>, 2015.

595 Jerrett, M., Burnett, R.T., Pope, C.A., Ito, K., Thurston, G., Krewski, D., Shi, Y., Calle, E., Thun, M.:
596 Long-term ozone exposure and mortality, *N. Engl. J. Med.*, 360, 1085–1095.
597 <https://doi.org/10.1056/NEJMoa0803894>, 2009.

598 Kawase, H., Nagashima, T., Sudo, K., Nozawa, T.: Future changes in tropospheric ozone under
599 representative concentration pathways (RCPs), *Geophys. Res. Lett.* 38, L05801.
600 <https://doi.org/10.1029/2010GL046402>, 2011.

601 Karset, I. H. H., Berntsen, T. K., Storelvmo, T., Alterskjær, K., Grini, A., Oliví, D., Kirkevåg, A., Seland,
602 Ø., Iversen, T., and Schulz, M.: Strong impacts on aerosol indirect effects from historical oxidant
603 changes, *Atmos. Chem. Phys.*, 18, 7669–7690, <https://doi.org/10.5194/acp-18-7669-2018>, 2018.

604 Kim, M.J., Park, R.J., Ho, C.-H., Woo, J.-H., Choi, K.-C., Song, C.-K., Lee, J.-B.: Future ozone and
605 oxidants change under the RCP scenarios, *Atmos. Environ.* 101, 103–115.
606 <https://doi.org/10.1016/J.ATMOSENV.2014.11.016>, 2015.

607 Kinnison, D. E., Brasseur, G. P., Walters, S., Garcia, R. R., Marsch, D. A., Sassi, F., Boville, B. A.,
608 Harvey, V. L., Randall, C. E., Emmons, L., Lamarque, J. F., Hess, P., Orlando, J. J., Tie, X. X.,
609 Randel, W., Pan, L. L., Gettelman, A., Granier, C., Diehl, T., Niemaier, U., and Simmons, A. J.:
610 Sensitivity of chemical tracers to meteorological parameters in the MOZART-3 chemical transport
611 model, *J. Geophys. Res.*, 112, D20302, <https://doi.org/10.1029/2006JD007879>, 2007.

612 Kleinman, I., Daum, P. H., Lee, Y.-N., Nunnermacker, L. J., Springston, S. R., Weinstein-Lloyd, J.,
613 Rudolph, J.: Ozone production efficiency in an urban area, *J. Geophys. Res.*, 107(D23), 4733,
614 <https://doi.org/10.1029/2002JD002529>, 2002.

615 Koffi, B., Dentener, F., Janssens-Maenhout, G., Guizzardi, D., Crippa, M., Diehl, T., Galmarini, S.,
616 Solazzo, E.: Hemispheric Transport Air Pollution (HTAP): Specification of the HTAP2 experiments–
617 Ensuring harmonized modelling, EUR 28255 EN, Luxembourg: Publications Office of the European
618 Union, <https://doi.org/10.2788/725244>, 2016.

619 Kong, L., Tang, X., Zhu, J., Wang, Z., Li, J., Wu, H., Wu, Q., Chen, H., Zhu, L., Wang, W., Liu, B.,
620 Wang, Q., Chen, D., Pan, Y., Song, T., Li, F., Zheng, H., Jia, G., Lu, M., Wu, L., and Carmichael, G.
621 R.: A 6-year-long (2013–2018) high-resolution air quality reanalysis dataset in China based on the
622 assimilation of surface observations from CNEMC, *Earth Syst. Sci. Data*, 13, 529–570,
623 <https://doi.org/10.5194/essd-13-529-2021>, 2021.

624 Lamarque, J.-F., Emmons, L. K., Hess, P. G., Kinnison, D. E., Tilmes, S., Vitt, F., Heald, C. L., Holland,
625 E. A., Lauritzen, P. H., Neu, J., Orlando, J. J., Rasch, P. J., and Tyndall, G. K.: CAM-chem:

626 description and evaluation of interactive atmospheric chemistry in the Community Earth System
627 Model, *Geosci. Model Dev.*, 5, 369–411, <https://doi.org/10.5194/gmd-5-369-2012>, 2012.

628 Lamarque, J.-F., Shindell, D.T., Josse, B., Young, P.J., Cionni, I., Eyring, V., Bergmann, D., Cameron-
629 Smith, P., Collins, W.J., Doherty, R., Dalsoren, S., Faluvegi, G., Folberth, G., Ghan, S.J., Horowitz,
630 L.W., Lee, Y.H., MacKenzie, I.A., Nagashima, T., Naik, V., Plummer, D., Righi, M., Rumbold, S.T.,
631 Schulz, M., Skeie, R.B., Stevenson, D.S., Strode, S., Sudo, K., Szopa, S., Voulgarakis, A., Zeng, G.:
632 The Atmospheric Chemistry and Climate Model Intercomparison Project (ACCMIP): overview and
633 de- scription of models, simulations and climate diagnostics, *Geosci. Model Dev.*, 6, 179–206,
634 <https://doi.org/10.5194/gmd-6-179-2013>, 2013.

635 Li, J., Nagashima, T., Kong, L., Ge, B., Yamaji, K., Fu, J. S., Wang, X., Fan, Q., Itahashi, S., Lee, H.-J.,
636 Kim, C.-H., Lin, C.-Y., Zhang, M., Tao, Z., Kajino, M., Liao, H., Li, M., Woo, J.-H., Kurokawa, J.,
637 Wang, Z., Wu, Q., Akimoto, H., Carmichael, G. R., and Wang, Z.: Model evaluation and
638 intercomparison of surface-level ozone and relevant species in East Asia in the context of MICS-Asia
639 Phase III – Part 1: Overview, *Atmos. Chem. Phys.*, 19, 12993–13015, [https://doi.org/10.5194/acp-](https://doi.org/10.5194/acp-19-12993-2019)
640 [19-12993-2019](https://doi.org/10.5194/acp-19-12993-2019), 2019.

641 Liu, G., Liu, J. J., Tarasick, D. W., Fioletov, V. E., Liu, J., Jin, J., Moeini, O., Sioris, C. E. and Osman,
642 M.: A global tropospheric ozone climatology from trajectory-mapped ozone soundings, *Atmos. Chem.*
643 *Phys.* 13, 10659-10675, <https://doi.org/10.5194/acp-13-10659-2013>, 2013.

644 Liu, J., Tarasick, D. W., Fioletov, V. E., McLinden C., Zhao, T., Gong, S., Sioris, C., Jin, J., Liu, G., and
645 Moeini, O.: A Global Ozone Climatology from Ozone Soundings via Trajectory Mapping: A
646 Stratospheric Perspective, *Atmos. Chem. Phys.*, 13, 11441-11464, [https://doi.org/10.5194/acp-13-](https://doi.org/10.5194/acp-13-11441-2013)
647 [11441-2013](https://doi.org/10.5194/acp-13-11441-2013), 2013.

648 Liu, Z., Doherty, R. M., Wild, O., O'Connor, F. M., and Turnock, S. T.: Tropospheric ozone changes and
649 ozone sensitivity from the present day to the future under shared socio-economic pathways, *Atmos.*
650 *Chem. Phys.*, 22, 1209–1227, <https://doi.org/10.5194/acp-22-1209-2022>, 2022.

651 Liu, Z., Wild, O., Doherty, R. M., O'Connor, F. M., and Turnock, S. T.: Benefits of Net Zero policies
652 for future ozone pollution in China, *EGUsphere* [preprint], [https://doi.org/10.5194/egusphere-2023-](https://doi.org/10.5194/egusphere-2023-230)
653 [230](https://doi.org/10.5194/egusphere-2023-230), 2023.

654 Lu, X., Zhang, L., and Shen, L.: Meteorology and Climate Influences on Tropospheric Ozone: a Review
655 of Natural Sources, Chemistry, and Transport Patterns, *Current Pollution Reports*, 5, 238–260,
656 <https://doi.org/10.1007/s40726-019-00118-3>, 2019.

657 Lu, X., Zhang, L., Wang, X., Gao, M., Li, K., Zhang, Y., Yue, X., and Zhang, Y.: Rapid Increases in
658 Warm-Season Surface Ozone and Resulting Health Impact in China since 2013, *Environ. Sci.*
659 *Technol. Lett.*, 7, 240–247, <https://doi.org/10.1021/acs.estlett.0c00171>, 2020.

660 Malley, C. S., Henze, D. K., Kuylenstierna, J. C. I., Vallack, H. W., Davila, Y., Anenberg, S. C., Turner,
661 M. C., Ashmore, M. R.: Updated global estimates of respiratory mortality in adults ≥ 30 Years of age
662 attributable to long-term ozone exposure, *Environ. Health Perspect*, 125, 87021,
663 <https://doi.org/10.1289/EHP1390>, 2017.

664 Myhre, G., Shindell, D., Breon, F.-M., Collins, W., Fuglestedt, J., Huang, J., Koch, D., Lamarque, J.-
665 F., Lee, D., Mendoza, B., Nakajima, T., Robock, A., Stephens, G., Takemura, T., Zhang, H.:
666 Anthropogenic and natural radiative forcing. In: *Climate Change 2013: the Physical Science Basis*.
667 Contribution of Working Group I to the Fifth Assessment Report of the Intergovernmental Panel on
668 Climate Change. Cambridge University Press, Cambridge, United Kingdom and New York, NY,
669 USA, 659-740, 2013.

670 Neale, R. B., Richter, J., Park, S., Lauritzen, P. H., Vavrus, S. J., Rasch, P. J., and Zhang, M.: The Mean
671 Climate of the Community Atmosphere Model (CAM4) in forced SST and fully coupled experiments,
672 *J. Climate*, 26, 5150–5168, <https://doi.org/10.1175/JCLI-D-12-00236.1>, 2013.

673 O'Connor, F. M., Johnson, C. E., Morgenstern, O., Abraham, N. L., Braesicke, P., Dalvi, M., Folberth,
674 G. A., Sanderson, M. G., Telford, P. J., Voulgarakis, A., Young, P. J., Zeng, G., Collins, W. J., Pyle,
675 J. A.: Evaluation of the new UKCA climate-composition model – Part 2: the Troposphere, *Geosci.*
676 *Model Dev.*, 7, 41–91, <https://doi.org/10.5194/gmd-7-41-2014>, 2014.

677 Oleson, K. W., Lawrence, D. M., Bonan, G. B., Flanner, M. G., Kluzek, E., Lawrence, P. J., Levis, S.,
678 Sean C. Swenson, S. C., Peter, E. T., Dai, A., Decker, M., Dickinson, R., Feddesma, J., Heald, C. L.,
679 Hoffman, F., Lamarque, J.-F., Mahowald, N., Niu, G.-Y., Qian, T., Randerson, J., Running, S.,
680 Sakaguchi, K., Slater, A., Stöckli, R., Wang, A., Yang, Z. L., Zeng, X.: Technical Description of
681 version 4.0 of the Community Land Model (CLM) (No. NCAR/TN-478+STR), University
682 Corporation for Atmospheric Research. <http://dx.doi.org/10.5065/D6FB50WZ>, 2010.

683 O'Neill, B. C., Kriegler, E., Riahi, K., Ebi, K. L., Hallegatte, S., Carter, T. R., Mathur, R., van Vuuren,
684 D. P.: A new scenario framework for climate change research: the concept of shared socioeconomic
685 pathways, *Clim. Change*, 122, 387–400, <https://doi.org/10.1007/s10584-013-0905-2>, 2014.

686 Rao, S., Klimont, Z., Smith, S.J., Dingenen, R. Van, Dentener, F., Bouwman, L., Riahi, K., Amann, M.,
687 Bodirsky, B.L., Van Vuuren, D.P., Reis, L.A., Calvin, K., Drouet, L., Fricko, O., Fujimori, S.,
688 Gernaat, D., Havlik, P., Harmsen, M., Hasegawa, T., Heyes, C., Hilaire, J., Luderer, G., Masui, T.,
689 Stehfest, E., Strefler, J., Van Der Sluis, S., Tavoni, M.: Future air pollution in the shared socio-
690 economic pathways, *Glob. Environ. Chang.*, 42, 346–358,
691 <https://doi.org/10.1016/j.gloenvcha.2016.05.012>, 2017.

692 Riahi, K., Van Vuuren, D.P., Kriegler, E., Edmonds, J., O'Neill, B.C., Fujimori, S., Bauer, N., Calvin,
693 K., Dellink, R., Fricko, O., Lutz, W., Popp, A., Cuaresma, J.C., Kc, S., Leimbach, M., Jiang, L., Kram,
694 T., Rao, S., Emmerling, J., Ebi, K., Hasegawa, T., Havlik, P., Humpenöder, F., Aleluia, L., Silva, D.,
695 Smith, S., Stehfest, E., Bosetti, V., Eom, J., Gernaat, D., Masui, T., Rogelj, J., Strefler, J., Drouet, L.,

696 Krey, V., Luderer, G., Harmsen, M., Takahashi, K., Baumstark, L., Doelman, J.C., Kainuma, M.,
697 Klimont, Z., Marangoni, G., Lotze-Campen, H., Obersteiner, M., Tabeau, A., Tavoni, M.: The Shared
698 Socioeconomic Pathways and their energy, land use, and greenhouse gas emissions implications: an
699 overview, *Glob. Environ. Chang.*, 42, 153–168, <https://doi.org/10.1016/j.gloenvcha.2016.05.009>,
700 2017.

701 Rienecker, M. M., Suarez, M. J., Gelaro, R., Todling, R., Bacmeister, J., Liu, E., Bosilovich, M. G.,
702 Schubert, S. D., Takacs, L., Kim, G.-K., Bloom, S., Chen, J., Collins, D., Conaty, A., da Silva, A.,
703 Gu, W., Joiner, J., Koster, R. D., Lucchesi, R., Molod, A., Owens, T., Pawson, S., Pegion, P., Redder,
704 C. R., Reichle, R., Robertson, F. R., Ruddick, A. G., Sienkiewicz, M., and Woollen, J.: MERRA:
705 NASA's Modern-Era Retrospective Analysis for Research and Application, *J. Climate*, 24, 3624–
706 3648, <https://doi.org/10.1175/JCLI-D-11-00015.1>, 2011.

707 Sander, S. P., Friedl, R. R., Barker, J. R., Golden, D. M., Kurylo, M. J., Sciences, G. E., Wine, P. H.,
708 Abbatt, J. P. D., Burkholder, J. B., Kolb, C. E., Moortgat, G. K., Huie, R. E., and Orkin, V. L.:
709 Chemical Kinetics and Photochemical Data for Use in Atmospheric Studies Evaluation Number 17
710 NASA Panel for Data Evaluation, *JLP Publ.*, 10–6, 2011.

711 Shi, X., Zheng, Y., Lei, Y., Xue, W., Yan, G., Liu, X., Cai, B., Tong, D., Wang, J.: Air quality benefits
712 of achieving carbon neutrality in China, *Sci. Total Environ.*, 795, 148784,
713 <https://doi.org/10.1016/j.scitotenv.2021.148784>, 2021.

714 Shindell, D. T., Faluvegi, G., Koch, D. M., Schmidt, G. A., Unger, N., and Bauer, S. E.: Improved
715 Attribution of Climate Forcing to Emissions, *Science*, 326, 716–718,
716 <https://doi.org/10.1126/science.1174760>, 2009.

717 Stevenson, D. S., Dentener, F. J., Schultz, M. G., Ellingsen, K., van Noije, T. P. C., Wild, O., Zeng, G.,
718 Amann, M., Atherton, C. S., Bell, N., Bergmann, D. J., Bey, I., Butler, T., Cofala, J., Collins, W. J.,
719 Derwent, R. G., Doherty, R. M., Drevet, J., Eskes, H. J., Fiore, A. M., Gauss, M., Hauglustaine, D.
720 A., Horowitz, L. W., Isaksen, I. S. A., Krol, M. C., Lamarque, J.-F., Lawrence, M. G., Montanaro,
721 V., Müller, J.-F., Pitari, G., Prather, M. J., Pyle, J. A., Rast, S., Rodriguez, J. M., Sanderson, M. G.,
722 Savage, N. H., Shindell, D. T., Strahan, S. E., Sudo, K., Szopa, S.: Multi-model ensemble simulations
723 of present-day and near future tropospheric ozone, *J. Geophys. Res.*, 111, D08301,
724 <https://doi.org/10.1029/2005JD006338>, 2006.

725 Stevenson, D. S., Young, P. J., Naik, V., Lamarque, J.-F., Shindell, D. T., Voulgarakis, A., Skeie, R. B.,
726 Dalsoren, S. B., Myhre, G., Berntsen, T. K., Folberth, G. A., Rumbold, S. T., Collins, W. J.,
727 MacKenzie, I. A., Doherty, R. M., Zeng, G., van Noije, T. P. C., Strunk, A., Bergmann, D., Cameron-
728 Smith, P., Plummer, D. A., Strode, S. A., Horowitz, L., Lee, Y. H., Szopa, S., Sudo, K., Nagashima,
729 T., Josse, B., Cionni, I., Righi, M., Eyring, V., Conley, A., Bowman, K. W., Wild, O., Archibald, A.:
730 Tropospheric ozone changes, radiative forcing and attribution to emissions in the atmospheric
731 chemistry and climate model Intercomparison project (ACCMIP), *Atmos. Chem. Phys.* 13, 3063–
732 3085. <https://doi.org/10.5194/acp-13-3063-2013>, 2013.

- 733 Sudo, K., Takahashi, M., and Akimoto, H.: Future changes in stratosphere-troposphere exchange and
734 their impacts on future tropospheric ozone simulations, *Geophys. Res. Lett.*, 30(24), 2256,
735 <https://doi.org/10.1029/2003GL018526>, 2003.
- 736 Tang, X., Zhu, J., Wang, Z. F., and Gbaguidi, A.: Improvement of ozone forecast over Beijing based on
737 ensemble Kalman filter with simultaneous adjustment of initial conditions and emissions, *Atmos.*
738 *Chem. Phys.*, 11, 12901–12916, <https://doi.org/10.5194/acp-11-12901-2011>, 2011.
- 739 Tang, X., Kong, L., Zhu, J., Wang, Z. F., Li, J. J., Wu, H. J., Wu, Q. Z., Chen, H. S., Zhu, L. L., Wang,
740 W., Liu, B., Wang, Q., Chen D. H., Pan Y. P., Song, T., Li, F., Zheng, H. T., Jia, G. L., Lu, M. M.,
741 Wu, L., and Carmichael, G. R.: A Six-year long High-resolution Air Quality Reanalysis Dataset over
742 China from 2013 to 2018, V2, *Sci. Data Bank*, <https://doi.org/10.11922/sciencedb.00053>, 2020a.
- 743 Tang, X., Kong, L., Zhu, J., Wang, Z. F., Li, J. J., Wu, H. J., Wu, Q. Z., Chen, H. S., Zhu, L. L., Wang,
744 W., Liu, B., Wang, Q., Chen D. H., Pan Y. P., Song, T., Li, F., Zheng, H. T., Jia, G. L., Lu, M. M.,
745 Wu, L., and Carmichael, G. R.: A Six-year long High-resolution Air Quality Reanalysis Dataset over
746 China from 2013 to 2018 (monthly and annual version), V1, *Sci. Data Bank*,
747 <https://doi.org/10.11922/sciencedb.00092>, 2020b.
- 748 Tie, X., Madronich, S., Walters, S., Edwards, D. P., Ginoux, P., Mahowald, N., Zhang, R. Y., Lou, C.,
749 Brasseur, G.: Assessment of the global impact of aerosols on tropospheric oxidants, *J. Geophys. Res.*,
750 110, D03204, <https://doi.org/10.1029/2004JD005359>, 2005.
- 751 Tilmes, S., Lamarque, J.-F., Emmons, L. K., Kinnison, D. E., Ma, P.-L., Liu, X., Ghan, S., Bardeen, C.,
752 Arnold, S., Deeter, M., Vitt, F., Ryerson, T., Elkins, J. W., Moore, F., Spackman, J. R., and Val
753 Martin, M.: Description and evaluation of tropospheric chemistry and aerosols in the Community
754 Earth System Model (CESM1.2), *Geosci. Model Dev.*, 8, 1395–1426, [https://doi.org/10.5194/gmd-](https://doi.org/10.5194/gmd-8-1395-2015)
755 8-1395-2015, 2015.
- 756 Tong, D., Cheng, J., Liu, Y., Yu, S., Yan, L., Hong, C., Qin, Y., Zhao, H., Zheng, Y., Geng, G., Li, M.,
757 Liu, F., Zhang, Y., Zheng, B., Clarke, L., and Zhang, Q.: Dynamic projection of anthropogenic
758 emissions in China: methodology and 2015–2050 emission pathways under a range of socio-
759 economic, climate policy, and pollution control scenarios, *Atmos. Chem. Phys.*, 20, 5729–5757,
760 <https://doi.org/10.5194/acp-20-5729-2020>, 2020.
- 761 Turnock, S. T., Wild, O., Sellara, A., O'Connor, F. M.: 300 years of tropospheric ozone changes using
762 CMIP6 scenarios with a parameterised approach. *Atmos. Environ.*, 213, 686–698,
763 <https://doi.org/10.1016/j.atmosenv.2019.07.001>, 2019.
- 764 Turnock, S. T., Wild, O., Dentener, F. J., Davila, Y., Emmons, L. K., Flemming, J., Folberth, G. A.,
765 Henze, D. K., Jonson, J. E., Keating, T. J., Kengo, S., Lin, M., Lund, M., Tilmes, S., O'Connor, F.
766 M.: The impact of future emission policies on tropospheric ozone using a parameterised approach,
767 *Atmos. Chem. Phys.*, 18, 8953–8978, <https://doi.org/10.5194/acp-18-8953-2018>, 2018.

768 Voulgarakis, A., Naik, V., Lamarque, J.-F., Shindell, D. T., Young, P. J., Prather, M. J., Wild, O., Field,
769 R. D., Bergmann, D., CameronSmith, P., Cionni, I., Collins, W. J., Dalsøren, S. B., Doherty, R. M.,
770 Eyring, V., Faluvegi, G., Folberth, G. A., Horowitz, L. W., Josse, B., MacKenzie, I. A., Nagashima,
771 T., Plummer, D. A., Righi, M., Rumbold, S. T., Stevenson, D. S., Strode, S. A., Sudo, K., Szopa, S.,
772 and Zeng, G.: Analysis of present day and future OH and methane lifetime in the ACCMIP
773 simulations, *Atmos. Chem. Phys.*, 13, 2563–2587, <https://doi.org/10.5194/acp-13-2563-2013>, 2013.

774 Wang, Y., Liao, H.: The impacts of transport from South and Southeast Asia on O₃ concentrations in
775 China from 2015 to 2050, *Chinese Science Bulletin (in Chinese)*, 67(18), 2043-2059,
776 <https://doi.org/10.1360/tb-2021-0707>, 2022.

777 Wang Y., Shen, L., Wu, S., Mickley, L., He, J., Hao, J.: Sensitivity of surface ozone over China to 2000–
778 2050 global changes of climate and emissions, *Atmos. Environ.*, 75, 374-382,
779 <https://doi.org/10.1016/j.atmosenv.2013.04.045>, 2013.

780 Wang, T., Wei, X. L., Ding, A. J., Poon, C. N., Lam, K. S., Li, Y. S., Chan, L. Y., and Anson, M.:
781 Increasing surface ozone concentrations in the background atmosphere of Southern China, 1994–
782 2007, *Atmos. Chem. Phys.*, 9, 6217–6227, <https://doi.org/10.5194/acp-9-6217-2009>, 2009.

783 Wang, Z. F., Sha, W. M., and Ueda, H.: Numerical modeling of pollutant transport and chemistry during
784 a high-ozone event in northern Taiwan, *Tellus B*, 52, 1189–1205, <https://doi.org/10.1034/j.1600-0889.2000.01064.x>, 2000.

786 Wild, O.: Modelling the global tropospheric ozone budget: exploring the variability in current models,
787 *Atmos. Chem. Phys.*, 7, 2643–2660, <https://doi.org/10.5194/acp-7-2643-2007>, 2007.

788 Wild, O. and Akimoto, H.: Intercontinental transport of ozone and its precursors in a three-dimensional
789 global CTM, *J. Geophys. Res.*, 106(D21), 27729-27744, <https://doi.org/10.1029/2000jd000123>, 2001.

790 Wild, O., Fiore, A. M., Shindell, D. T., Doherty, R. M., Collins, W. J., Dentener, F. J., Schultz, M. G.,
791 Gong, S., MacKenzie, I. A., Zeng, G., Hess, P., Duncan, B. N., Bergmann, D. J., Szopa, S., Jonson,
792 J. E., Keating, T. J., and Zuber, A.: Modelling future changes in surface ozone: a parameterized
793 approach, *Atmos. Chem. Phys.*, 12, 2037–2054, <https://doi.org/10.5194/acp-12-2037-2012>, 2012.

794 Xu, B., Wang, T., Ma, D., Song, R., Zhang, M., Gao, L., Li, S., Zhuang, B., Li, M., Xie, M.: Impacts of
795 regional emission reduction and global climate change on air quality and temperature to attain carbon
796 neutrality in China, *Atmos. Res.*, <https://doi.org/10.1016/j.atmosres.2022.106384>, 2022.

797 Yang, X. L., Zhou, B. T., Xu, Y., and Han, Z.-Y.: CMIP6 Evaluation and Projection of Temperature and
798 Precipitation over China, *Adv. Atmos. Sci.*, 38(5), 817–830, <https://doi.org/10.1007/s00376-021-0351-4>, 2021.

800 Young, P. J., Archibald, A. T., Bowman, K. W., Lamarque, J.-F., Naik, V., Stevenson, D. S., Tilmes, S.,
801 Voulgarakis, A., Wild, O., Bergmann, D., Cameron-Smith, P., Cionni, I., Collins, W. J., Dalsøren, S.

802 B., Doherty, R. M., Eyring, V., Faluvegi, G., Horowitz, L. W., Josse, B., Lee, Y. H., MacKenzie, I.
803 A., Nagashima, T., Plummer, D. A., Righi, M., Rumbold, S. T., Skeie, R. B., Shindell, D. T., Strode,
804 S. A., Sudo, K., Szopa, S., and Zeng, G.: Pre-industrial to end 21st century projections of tropospheric
805 ozone from the Atmospheric Chemistry and Climate Model Intercomparison Project (ACCMIP),
806 *Atmos. Chem. Phys.*, 13, 2063–2090, <https://doi.org/10.5194/acp-13-2063-2013>, 2013.

807 Young, P. J., Naik, V., Fiore, A. M., Gaudel, A., Guo, J., Lin, M. Y., Neu, J. L., Parrish, D. D., Rieder,
808 H. E., Schnell, J. L., Tilmes, S., Wild, O., Zhang, L., Ziemke, J., Brandt, J., Delcloo, A., Doherty, R.
809 M., Geels, C., Hegglin, M. I., Hu, L., Im, U., Kumar, R., Luhar, A., Murray, L., Plummer, D.,
810 Rodriguez, J., Saiz-Lopez, A., Schultz, M. G., Woodhouse, M. T., Zeng, G.: Tropospheric Ozone
811 Assessment Report: Assessment of global-scale model performance for global and regional ozone
812 distributions, variability, and trends, *Elem. Sci. Anth.*, 6, 10, <https://doi.org/10.1525/elementa.265>,
813 2018.

814 Zanis, P., Akritidis, D., Turnock, S., Naik, V., Szopa, S., Georgoulias, A. K., Bauer, S. E., Deushi, M.,
815 Horowitz, L. W., Keeble, J., Sager, P. L., O'Connor, F. M., Oshima, Naga., Tsigaridis, K. and Noije,
816 T.: Climate change penalty and benefit on surface ozone: A global perspective based on CMIP6 Earth
817 system models, *Environ. Res. Lett.*, 17, 024014, <https://doi.org/10.1088/1748-9326/ac4a34>, 2022.

818 Zaveri, R. A., Berkowitz, C. M., Kleinman, L. I., Springston, S. R., Doskey, P. V., Lonneman, W. A.,
819 Spicer, C. W.: Ozone production efficiency and NO_x depletion in an urban plume: Interpretation of
820 field observations and implications for evaluating O₃-NO_x-VOC sensitivity, *J. Geophys. Res.*,
821 108(D14), 4436, <https://doi.org/10.1029/2002JD003144>, 2003.

822 Ziemke, J. R., Chandra, S., Labow, G. J., Bhartia, P. K., Froidevaux, L., and Witte, J. C.: A global
823 climatology of tropospheric and stratospheric ozone derived from Aura OMI and MLS measurements,
824 *Atmos. Chem. Phys.*, 11, 9237–9251, <https://doi.org/10.5194/acp-11-9237-2011>, 2011.

825 Zhu, J. and Liao, H.: Future ozone air quality and radiative forcing over China owing to future changes
826 in emissions under the Representative Concentration Pathways (RCPs), *J. Geophys. Res.: Atmos.*,
827 121, 1978 – 2001, <https://doi.org/10.1002/2015JD023926>, 2016.